Dynamic events in rocks / rockmasses

Autor: Prof. Dr. habil. Heinz Konietzky, Dr. Christian Jakob & Mr. Jian Zhao
(TU Bergakademie Freiberg, Geotechnical Institute)

1   Introduction

All geomechanical processes are time-dependent i.e. dynamic. Only process velocities vary strongly. There are highly dynamic processes like explosions with propagation speeds of several 1000 m/s and extremely slow elapsing processes like orogenesis or creep processes with velocities in order of mm/year.

According to the length of the observation window processes can be treated as real dynamic or quasi-static: Thus if change of physical quantities in the observation window is insignificant low, a static view can be carried out.

In many cases processes interfere with each other, where velocities and magnitudes can be very different (e.g. a blast event at digging in a creeping salt rock). That is why it must be decided in every individual case how these coupled processes have to be considered.

For practical reasons in geomechanics often just the "highly dynamic" ones are meant by dynamic processes in contrast to the slowly elapsing ones, usually covered by the definition "creep".

Tab. 1.1 shows an overview of significant geomechanical relevant dynamic processes.

Tab. 1.1: Dynamic processes in hard rocks

Dynamic process	Duration	Occurrence	Remarks
Earthquakes	Seconds to minutes	Shocks, rifts, cracks, faults	at plate edges, intra plate seismicity
Blasts, explosions	Seconds	Shocks, fractures	because of mining, tunnel excavation and military
Induced seismicity	Seconds to minutes	Shocks, fractures	dam-, mining-, injection-, reservoir induced and fracturing
Recent crust movements	Millions of years	plate tectonics, trench formation, orogenesis	mm/year
Depression events at earth surface	Minutes to years	Earth fall, geosyncline	up to several m surface deep and several km^2 big
Mass movements	Minutes	Rockslide, mudflow avalanches	into the km^3 range
Dynamic events in rock and tunnel construction and mining	Seconds to days	Rock burst, fractures	triggers micro-earthquakes and earthquakes up to $M \approx 5$

2   Introduction to seismology

Dynamic events in the earth generate different kinds of elastic waves. The different types of waves differ in propagation velocity, amplitude and frequency. Fig. 2.1 shows a seismological record, in which body waves (P and S) as well as surface waves (Rayleigh and Love) are visible.
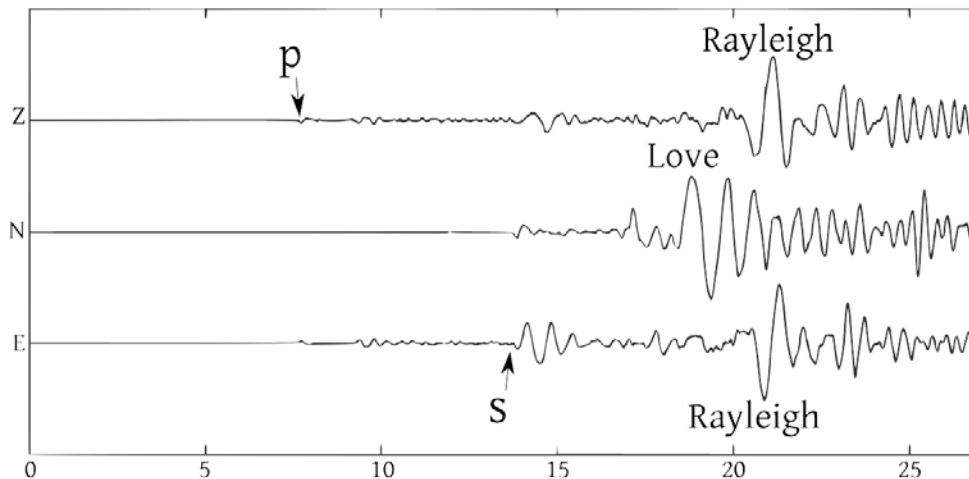

Fig. 2.1: Example seismological record (Meier: http://www.ifg.uni-kiel.de)

From the records of worldwide installed seismometers seismologists can characterize the source (explosion, landslide, earthquake, mine collapse, meteor impact etc.) and determine source parameters (hypocentre, source time, magnitudes, source mechanism etc.).

2.1   Characteristics of elastic waves

During propagation in a media elastic waves dissipate energy. The dissipation differentiates between geometrical spreading, damping and scattering. Surface waves propagate only at the surface of a media, accordingly in two dimensions. Body waves propagate in three dimensions in the media. Consequently the energy dissipation from geometrical spreading of surface waves is smaller and the range of influence is bigger than that of body waves.

The damping of elastic waves is frequency dependent. High frequencies are damped stronger than low frequencies. This is the reason for the frequency spectra change of the wave depending on travelled distance in a media.

2.1.1   Body waves

The P-Wave (primary wave or also called pressure wave or longitudinal wave) is characterized by high frequencies and high propagation velocities. Because of the stronger damping of this high frequency waves they mostly have smaller amplitudes than other waves. The oscillation of particles in the media take place in the direction of propagation (see Fig. 2.2).

Dynamic events in rocks / rockmasses

Only for private and internal use!   Updated: 16 September 2021
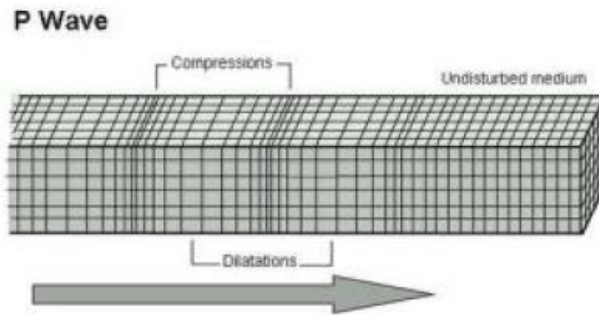
P Wave

Fig. 2.2: P-wave

P-waves propagate in all media (solids, liquids and gases). Depending on the density of a media the propagation velocity varies between 343 m/s (acoustic waves in air) and ~ 13700 m/s in the lower mantle of the earth. Selected values of propagation velocity for rocks and sediments are shown in Tab. 2.1.

Tab. 2.1: Typical propagation velocities for P- and S-waves in rocks and soils (sediments)

material	v_p in km/s	v_s in km/s	material	v_p in km/s	v_s in km/s
air	0.3	-	water	1.5	-
sediments			metamorphic		
clay	1.2 - 2.8	0.11 - 1.5	gneiss	6.6 – 7.0	3.4 – 4.0
loam	0.5 - 1.9	0.44 - 1.08	amphibolite	6.9 – 7.0	3.8 - 4.6
marl	1.2 - 4.7	0.4 - 2.6	peridotite	7.9 - 8.1	4.2 - 4.7
sand*	0.1 - 0.6	0.1 - 0.5	eclogite	7.8 - 8.1	4.5 – 5.0
sand**	0.2 – 2.0	0.1 - 0.5	magmatic		
gravel*	0.6 - 1.4	0.32 - 0.7	granite	5.6 - 6.3	2.5 - 3.8
sandstone	0.8 - 4.5	0.32 - 2.7	gabbro	6.5 - 6.8	3.8 - 3.9
limestone	2.0 - 6.2	1.8 - 3.8	basalt	5.5 - 6.3	n. a.
claystone	2.2 - 4.2	0.42 - 0.8	* (dry) ** (wet)		

The propagation velocity for P-waves is given by the elasticity parameters (elasticity modulus E and Poisson's ratio v) and the density ρ. With the Lamé parameters

$$\lambda = \frac{vE}{(1+v)(1-2v)} \quad \text{and} \quad \mu = \frac{E}{2(1+v)} \tag{2.1}$$

the P-wave velocity is resulting in

$$v_p = \sqrt{\frac{\lambda + 2\mu}{\rho}} \tag{2.2}$$

The S-Wave (secondary wave or also called transverse wave or shear wave) has lower frequencies and lower propagation velocities than the P-wave. Normally the S-wave has a higher amplitude than the P-wave. The oscillation of particles in the media take place orthogonally to the direction of propagation (see Fig. 2.3).
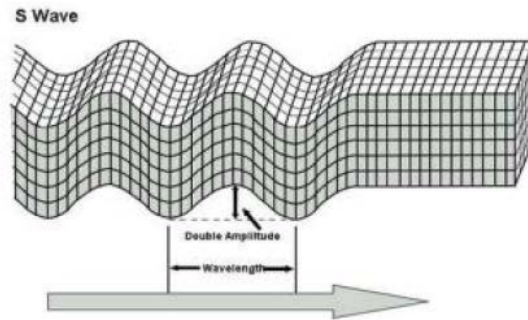
Fig. 2.3: S-wave

S-waves propagate only in media which have a shear modulus $G = \mu > 0$ and hence have a shear resistance. For that reason shear waves cannot propagate in liquids and gases. The S-Wave velocity is determined by μ and ρ as follows.

$$v_s = \sqrt{\frac{\mu}{\rho}}$$
(2.3)

As an approximation the S-wave velocity can determined by the ratio $V_p / V_s \approx \sqrt{3}$.

2.1.2 Surface waves

Surface waves are generated by refraction of P- and S-waves at all free surfaces (huge impedance contrast). Rayleigh-waves, named by the British physicist John William Rayleigh (1842-1919), are characterized by low frequencies (around 0.05 Hz) and high amplitudes. The oscillation of particles in the media is elliptically on a vertical plain (see Fig. 2.4).
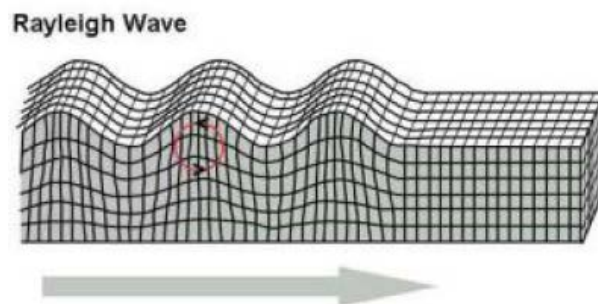
Fig. 2.4: Rayleigh-wave

The propagation velocity is with 2 - 4 km/s a bit smaller than the S-wave velocity. Water waves at the surface of a sea or an ocean are typical Rayleigh-waves. Rayleigh-waves triggered from earthquakes felt most strongly and cause the most damage.

Love-waves, named by the British mathematician Augustus Edward Hough Love (1863 - 1940), are also characterized by low frequencies and high amplitudes. The oscillation of particles in the media is horizontal, perpendicular to the direction of movement (see Fig. 2.5).

Dynamic events in rocks / rockmasses

Only for private and internal use!   Updated: 16 September 2021
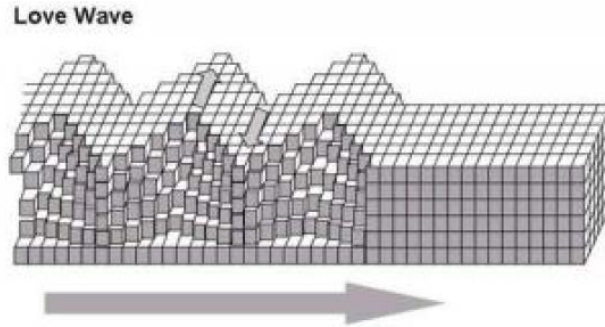
Love Wave

Fig. 2.5: Love-wave

They are with 2 - 4.4 km/s the fastest surface waves, but still slower than S-Waves. Love-waves generated from earthquakes can cause damage by horizontal shearing of the soil.

2.2 Localization of earthquakes

The localization of an earthquake consists of the determination of spatial location of the source (x, y, z or depth and corresponding projection to the surface) and source time of the earthquake. To determine this parameters the arrival times (t_p and t_s) from P-waves and S-waves are used.

2.2.1 Absolute localization

The analysis of the differences in wave runtime is denominating the absolute localization. This method for local earthquakes presumes a homogeneous and isotropic half space. The model concept supposes a punctate rupture (hypocenter with coordinates x_0, y_0, z_0) in the rock at the time t_0. The source emits seismic waves spherical with the velocities V_p respectively V_s and hit the seismic stations (seismometers or geophones) i at the times t_i. With the coordinates (x_i, y_i, z_i) the station locations are termed. If the arrival time of P-wave and S-wave $t_{p,i}$ und $t_{s,i}$ can be determined, then the source time t_0 and the hypocentre distance D_i to the station can also by determined.

$$v_p = \frac{D_i}{t_{p,i} - t_0} \text{ and } v_s = \frac{D_i}{t_{s,i} - t_0} \tag{2.4}$$

Equations in (2.4) result in the relation between runtime difference $t_{s,i} - t_{p,i}$ and source time.

$$t_{s,i} - t_{p,i} = \left(\frac{v_p}{v_s} - 1 \right) \left(t_{p,i} - t_0 \right) \tag{2.5}$$

From equations (2.4) and (2.5) the source time can be determined by

$$t_0 = t_{p,i} - \frac{t_{s,i} - t_{p,i}}{\frac{v_p}{v_s} - 1} \tag{2.6}$$

Dynamic events in rocks / rockmasses

Only for private and internal use!   Updated: 16 September 2021

and the hypocenter distance D_i to the station i by

$$D_i = v_p \left(t_{p,i} - t_0 \right) \tag{2.7}$$

In general, P-wave onsets are allocable more exactly than S-wave onsets from the seismograms. For this reason most locating algorithms use P-wave onsets preferential. The theoretical onset time result from geometric considerations as follows.

$$t_{theo.} = \frac{D_i}{v} = \frac{\sqrt{\left(x_i - x_0 \right)^2 + \left(y_i - y_0 \right)^2 + \left(z_i - z_0 \right)^2}}{v} \tag{2.8}$$

Thereby is V the propagation velocity of the P-wave or the S-wave. The measured runtime

$$t_{meas.} = t_i - t_0 \tag{2.9}$$

differs normally from the theoretical value $t_{theo.}$. Hence the difference is

$$\Delta t = t_{meas.} - t_{theo.} \neq 0 \tag{2.10}$$

because the propagation velocity is not homogeneous in the ground and the onsets are not exactly allocable. Using equations (2.8) and (2.9) in equation (2.10) results in the Geiger equation (named by the Swiss geophysicist Ludwig Carl Geiger).

$$\Delta t = t_i - t_0 - \frac{\sqrt{\left(x_i - x_0 \right)^2 + \left(y_i - y_0 \right)^2 + \left(z_i - z_0 \right)^2}}{v} \tag{2.11}$$

For solving the equation system the least square method is used, that means it becomes a minimization problem (Künzel 2013).

$$\frac{1}{N} \sum_{i=1}^{N} \left[t_i - t_0 - \frac{\sqrt{\left(x_i - x_0 \right)^2 + \left(y_i - y_0 \right)^2 + \left(z_i - z_0 \right)^2}}{v} \right]^2 \Rightarrow Min \tag{2.12}$$

This minimization problem is solved by giving a start value and find the minimum iteratively (Schulte-Theis 1995). Equation (2.11) contains four unknowns (x_0, y_0, z_0 und t_0). For this reason at least four onsets of P- and S-waves from at least three stations are necessary for localization. Fig. 2.6 shows the overlap of three hemispheres with the radius D_i.
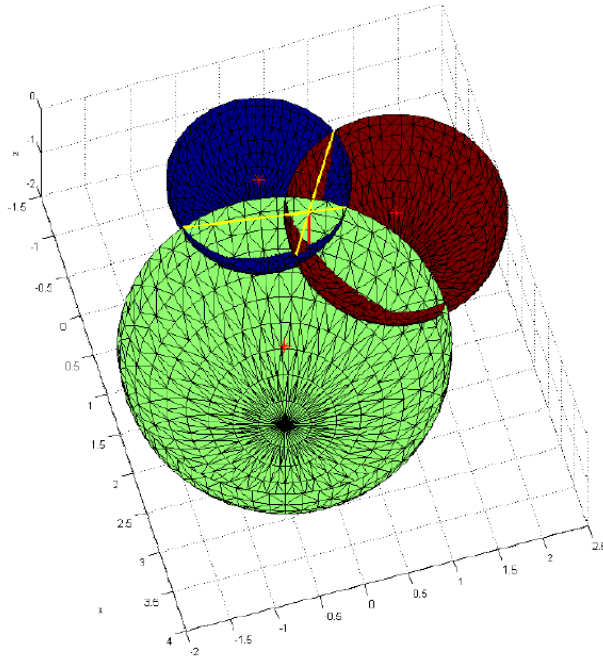
Dynamic events in rocks / rockmasses

Only for private and internal use!   Updated: 16 September 2021

Fig. 2.6: Localization of an earthquake with three stations (http://www.geophysik.uni-muenchen.de/)

2.2.2 Relative localization

A relative localization can be used to improve the distribution resolution from nearby events. In this process a relocation with the results of the absolute localization is performed. Thereby the runtime of different earthquakes is compared to get more accurate results. To perform relative localization, an absolute reference point is necessary. For the Master-Event-Technique a well localized earthquake or a performed blast is used for that. For the Joint Hypocenter Determination (JHD) the focal point of all hypocentres is used instead. Both methods can be combined with a waveform correlation (Waldhauser 2010). The relative localization error can be reduced significantly with this methods (see
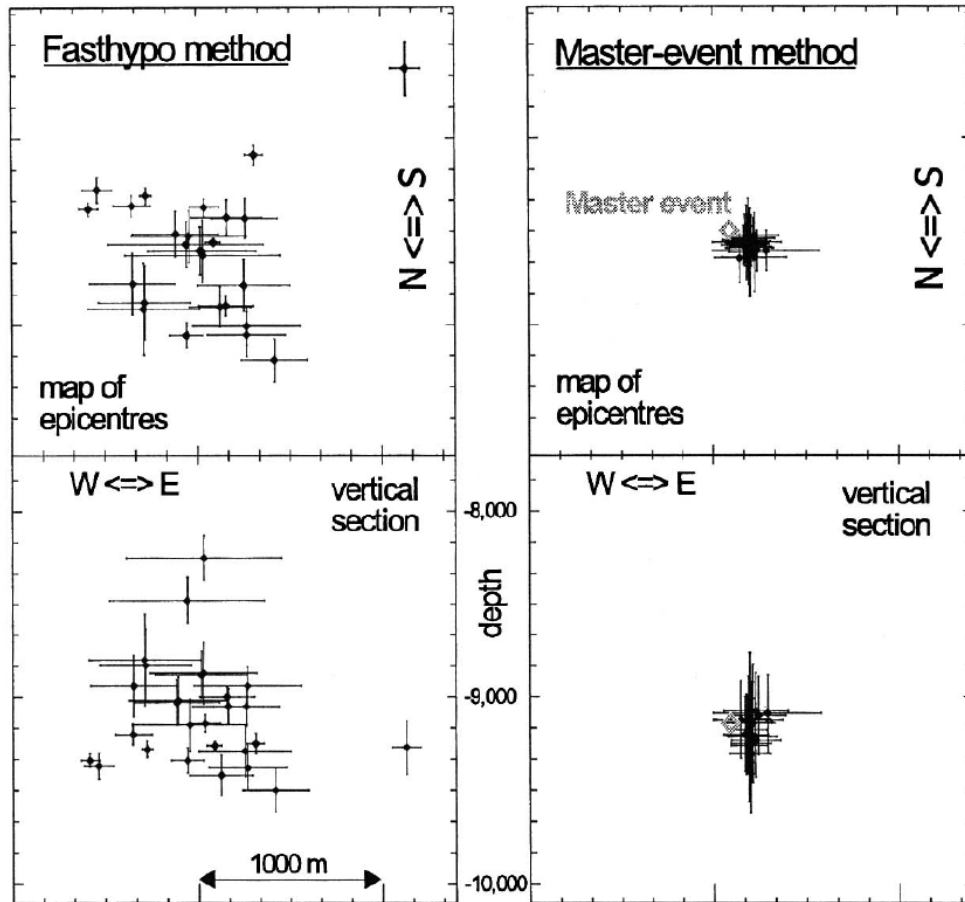Fig. 2.7).

Fig. 2.7: Comparison of localization accuracy of absolute (left) and relative localization (right) (Fischer & Horálek, 2000)

2.3 Magnitudes and intensities

Magnitudes are normally related to maximum amplitudes of the seismograms and therefore they are related to the released energy of an earthquake. A well known magnitude is the local magnitude M_L also called Richter-magnitude. Charles Richter (1900 - 1985) realized the correlation between measured amplitude A and the epicentre distance Δ and found the following relation.

$$\frac{A(\Delta)}{A_0(\Delta)} = constant \tag{2.13}$$

A_0 denotes the amplitude of a reference earthquake. In doing so the reference earthquake in a distance of $\Delta = 100$ km and an amplitude of $A_0 = 1$ mm in California is defined by Richter as magnitude $M_L = 3$. The local magnitude is given by equation (2.14).

$$M_L = \log A(\Delta) - \log A_0(\Delta) \tag{2.14}$$

Equation (2.14) is valid for epicentre distances Δ < 600 km only. The local magnitude has an upper limit of M_L = 6.5 which is caused by measurement devices. Larger magnitudes are determined by moment magnitudes.

The moment magnitude M_w is based on the concept of the seismic moment M_0 and is calculated as follows.

$$M_w = \frac{2}{3}\left(\log M_0 - 9.1\right) \text{ (for } M_0 \text{ in Joule)} \tag{2.15}$$

The seismic moment is a measure for the strength of the earthquake and is composed of rocks shear modulus G, the rupture area A and the displacement D along F (see also section 3).

$$M_0 = G \cdot A \cdot D \text{ (scalar)} \tag{2.16}$$

To determine the surface wave magnitude M_s the peak ground velocity $(A/T)_{max}$ is used.

$$M_s = \log\left(A/T\right)_{max} + 1.66\log\Delta + 3.3 \tag{2.17}$$

The Moscow-Prague-equation (2.17) is valid for epicentre distances between 2° and 160° and hypocentre depths up to 50 km. The surface wave magnitude scale is limited at M_s = 8.5.

For the body wave magnitude M_b (also m_b or m_B) the peak ground velocity $(A/T)_{max}$ of P- and S-waves is used.

$$M_b = \log\left(A/T\right)_{max} + Q\left(\Delta, h\right) \tag{2.18}$$

Where Q is the correcting term which depends on epicentre distance, depth h and the used instrument. The body wave magnitude scale is valid up to M_b = 6.5. Tab. 2.2 gives an overview about seismic events in terms of magnitude, occurrence per year and released energy.

Tab. 2.2: Magnitude scale with description, released energy (TNT-equivalent in [t] and in [J]) and the average frequency of occurrence per year

Magnitude	Description	Released energy		Occurrence
0.1 - 1.9	Micro	0.006 to 1 t	0.002 to 4.2 GJ	> 2,500,000
2.0 - 2.9	Minor	1 to 32 t	4.2 to 135 GJ	350,000
3.0 - 3.9	Minor	32 to 1,000 t	135 to 4,200 GJ	49,000
4.0 - 4.9	Light	1 to 32 kt	4.2 to 135 TJ	6,200
5.0 - 5.9	Moderate	32 to 1,000 kt	135 to 4,200 TJ	800
6.0 - 6.9	Strong	1 to 50 Mt	4.2 to 210 PJ	120
7.0 - 7.9	Very strong	50 to 1,000 Mt	210 to 4,200 PJ	18
8.0 - 8.9	Disastrous	1 to 5.6 Gt	4.2 to 23.5 EJ	1
9.0 - 9.9	Catastrophic	5.6 to 1,000 Gt	23.5 to 4,200 EJ	0.05
10.0 - ∞	Ruinous	> 1 Gt	> 4,200 EJ	0.01

Dynamic events in rocks / rockmasses

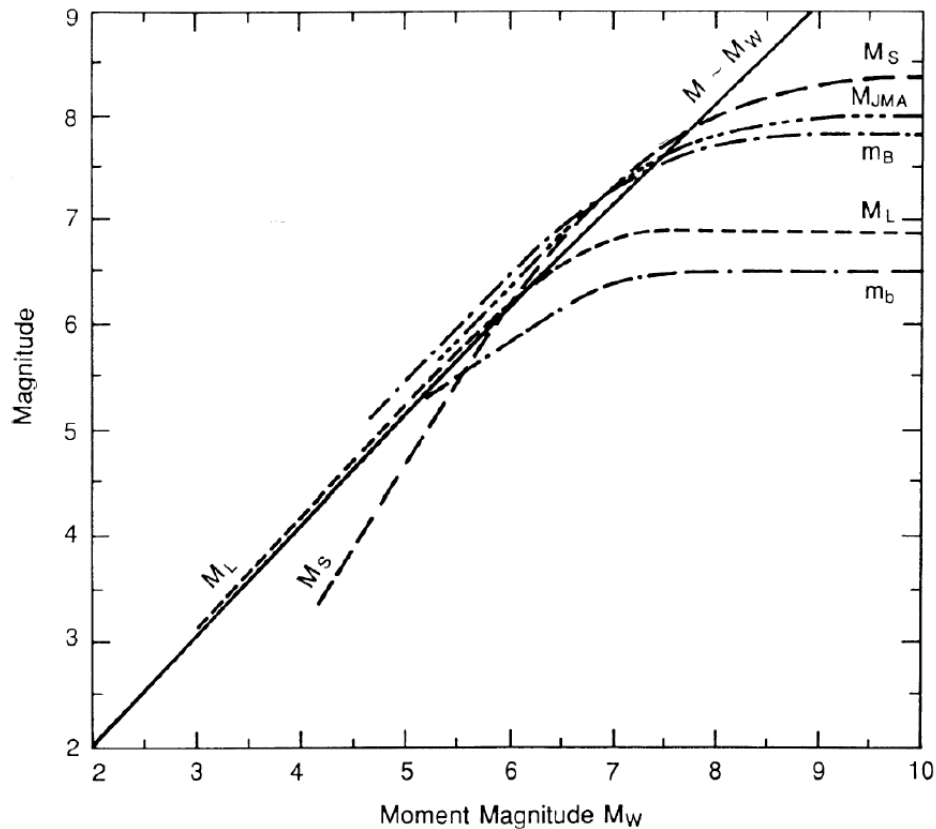Only for private and internal use!   Updated: 16 September 2021

Fig. 2.8: Comparison of moment magnitude with other magnitudes (Studer & Koller, 1997)

The intensity is also a measure for the strength of an earthquake. It describes the observed effects of an earthquake at the ground surface without measurement devices (Studer and Koller 1997). These effects are damages at buildings and human feelings (macro seismic). In contrast to a magnitude, multiple intensity values exist for one earthquake depending on the epicentre distance.

There are different scales of intensity. Most of them are divided in twelve steps usually numbered by roman digits. The most common scales are the European Macroseismic Scale (EMS-98), the Modified Mercalli Scale (MMS) and the Rossi-Forel-Scale. Fig. 2.9 shows the EMS-98 in short form.

Dynamic events in rocks / rockmasses

Only for private and internal use!   Updated: 16 September 2021

EMS intensity	Definition	Description of typical observed effects (abstracted)
I	Not felt	Not felt.
II	Scarcely felt	Felt only by very few individual people at rest in houses.
III	Weak	Felt indoors by a few people. People at rest feel a swaying or light trembling.
IV	Largely observed	Felt indoors by many people, outdoors by very few. A few people are awakened. Windows, doors and dishes rattle.
V	Strong	Felt indoors by most, outdoors by few. Many sleeping people awake. A few are frightened. Buildings tremble throughout. Hanging objects swing considerably. Small objects are shifted. Doors and windows swing open or shut.
VI	Slightly damaging	Many people are frightened and run outdoors. Some objects fall. Many houses suffer slight non-structural damage like hair-line cracks and fall of small pieces of plaster.
VII	Damaging	Most people are frightened and run outdoors. Furniture is shifted and objects fall from shelves in large numbers. Many well built ordinary buildings suffer moderate damage: small cracks in walls, fall of plaster, parts of chimneys fall down; older buildings may show large cracks in walls and failure of fill-in walls.
VIII	Heavily damaging	Many people find it difficult to stand. Many houses have large cracks in walls. A few well built ordinary buildings show serious failure of walls, while weak older structures may collapse.
IX	Destructive	General panic. Many weak constructions collapse. Even well built ordinary buildings show very heavy damage: serious failure of walls and partial structural failure.
X	Very destructive	Many ordinary well built buildings collapse.
XI	Devastating	Most ordinary well built buildings collapse, even some with good earthquake resistant design are destroyed.
XII	Completely devastating	Almost all buildings are destroyed.

Fig. 2.9: Short form of EMS-98

Dynamic events in rocks / rockmasses

Only for private and internal use!   Updated: 16 September 2021

2.4 Seismotectonics

Seismotectonics describes the earthquake origin with focus on movements and deformations of the earth's crust. The American geophysicist Harry Fielding Reid (1859 - 1944) developed the elastic rebound theory that implies that stresses in the earth's crust are discharging jerkily in form of earthquakes along pre-existing faults. The conceptual model is a shear fracture like shown in
Fig. 2.10. With growing stress the strength of the rock is exceeded at a certain point and it comes to a fracture or slip along the shear plane.
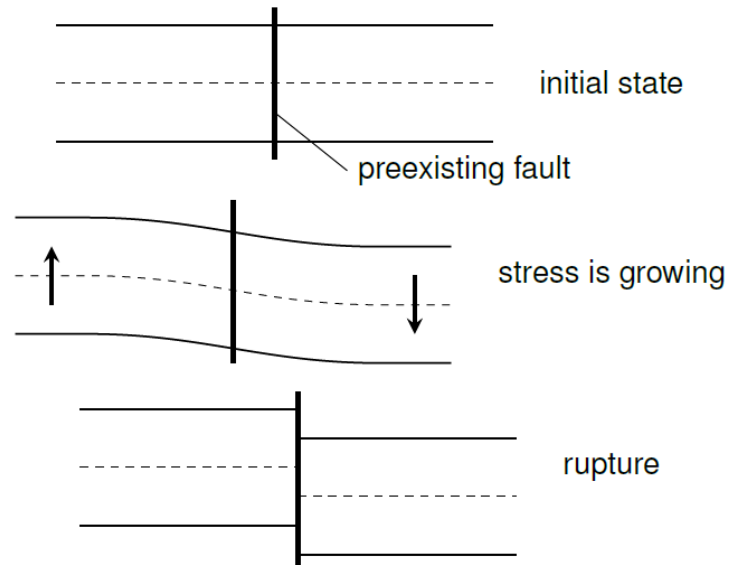
Fig. 2.10: Elastic rebound theory

A black dot (see Fig. 2.11) tags the hypocentre of the earthquake. The movement of the rupture front around the hypocentre is pointed by the time steps t_1 and t_2. The displacement field is indicated by the small arrows.
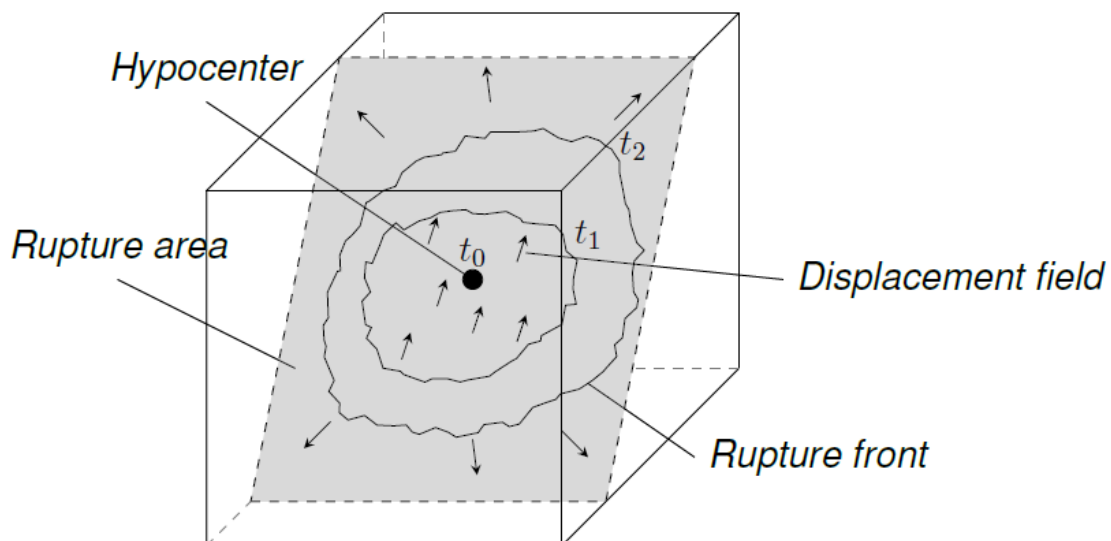
Fig. 2.11: Rupture area in a volume

2.5   Determination of source parameters

2.5.1   Fault plane solution

P-wave polarities of the vertical component (*z*) are picked from seismometer recordings. This happens already during picking the onsets. Imagine a hypothetic sphere around the earthquake focus (see Fig. 2.12). The penetration points of ray paths to the stations are marked on the spheres surface.

A peak upwards means a compressive onset and is denoted by C. In contrast a movement downwards is a dilative onset and is denoted by D. The penetration points are marked by C or D respectively their onset (see Fig. 2.13 left). In doing so quadrants with same polarities develop, which are separated by big circular curves (see Fig. 2.13, middle). After convention of Aki & Richards compressive onsets are coloured in black or any other (dark) colour and dilative onsets in white or any other (light) colour (Fig. 2.13 right). If many points are located in the transition zones of C to D, both areas can be exactly separated and a very accurate fault plane solution can be achieved. That is why many station recordings are needed for this method.
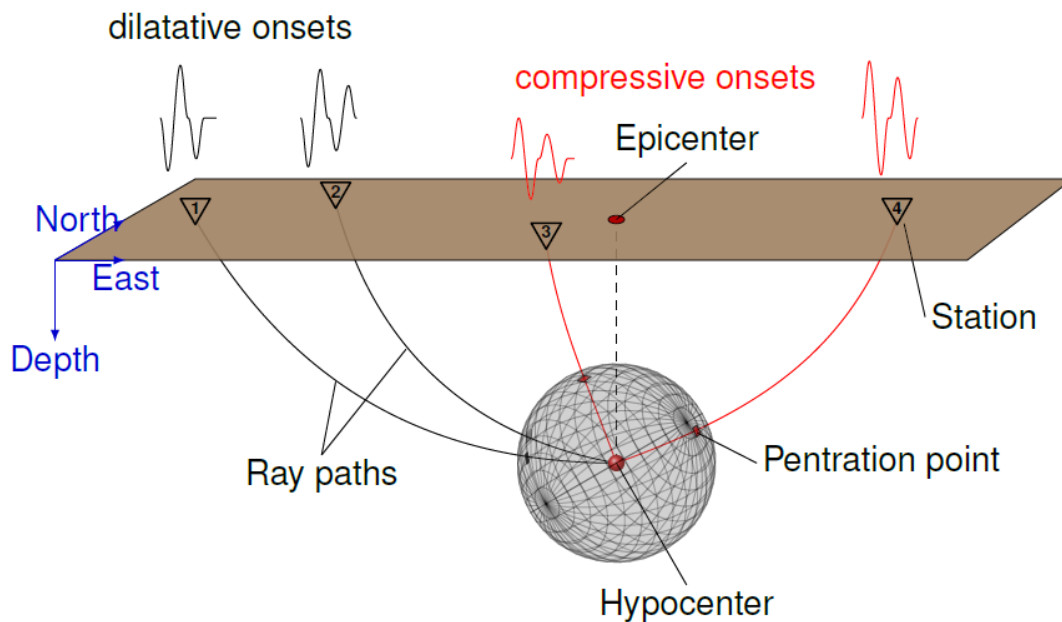

Fig. 2.12: Earthquake focus with hypothetic sphere and penetration points of the ray paths (red: compressive, black: dilative) to the stations

(a) mark onsets   (b) plot circles   (c) color quadrants
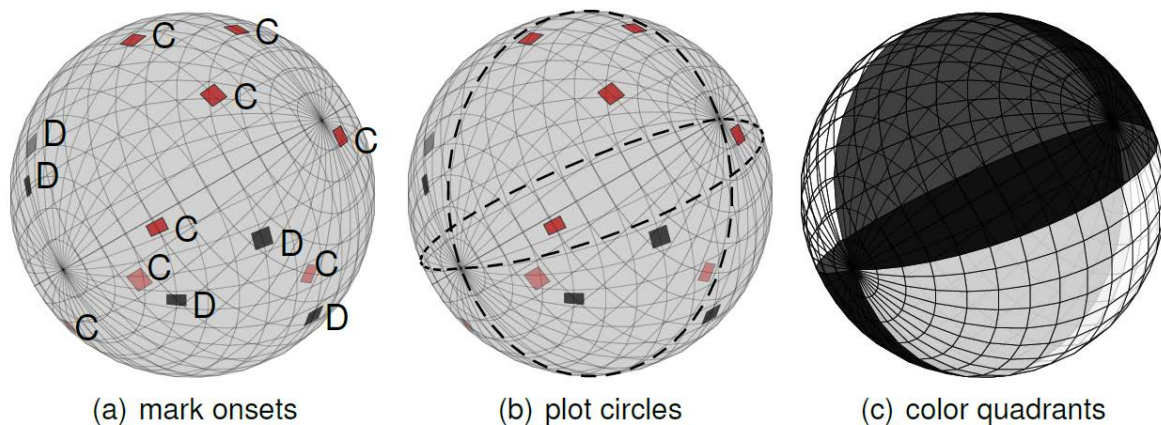
Fig. 2.13: Evolution of a fault plane solution by the onset method

With this method good results can just be obtained, when a sufficient amount of polarities are available and when they are well distributed over the sphere surface. This means that this method can be used for earthquakes with big magnitudes. To determine fault plane solutions of smaller earthquakes with less polarities, additional information like amplitude ratios are necessary.

A fault plane solution is usually illustrated by an azimuthal equal-area projection (also called Lambert azimuthal projection or Schmidt net) of the lower hemisphere.
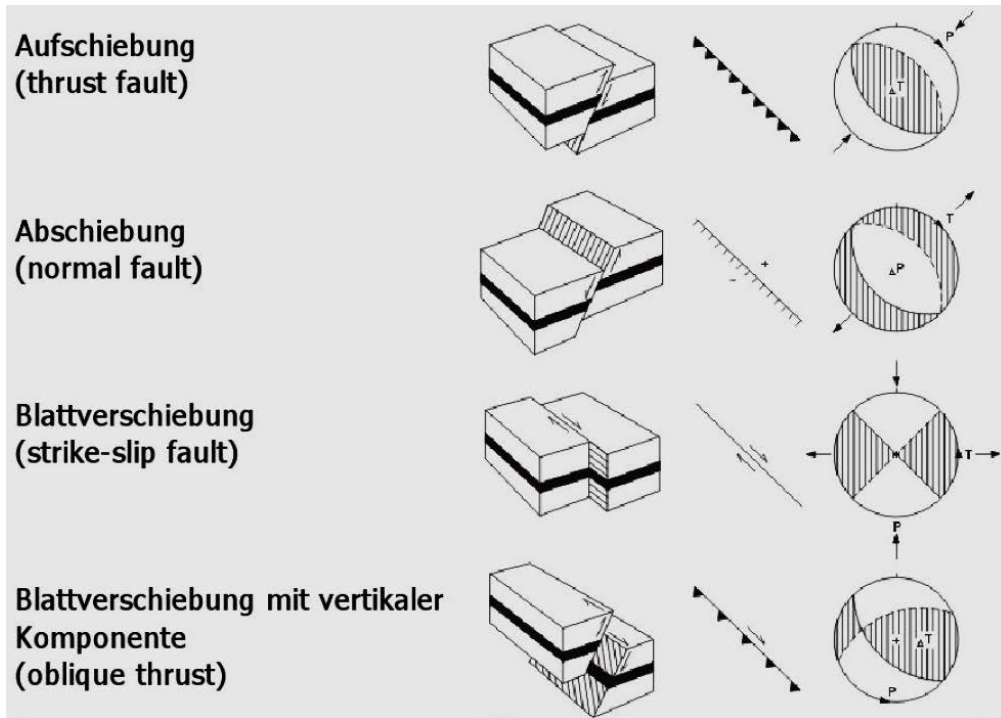

Fig. 2.14: Different fault types with corresponding fault plane solutions (Berckhemer, 1990)

Fig. 2.15 illustrates the radiation pattern for a double couple source (simplest representation of fault slip, see also section 3). Note, that fault plane solution provides always two potential fault planes (no unique solution).
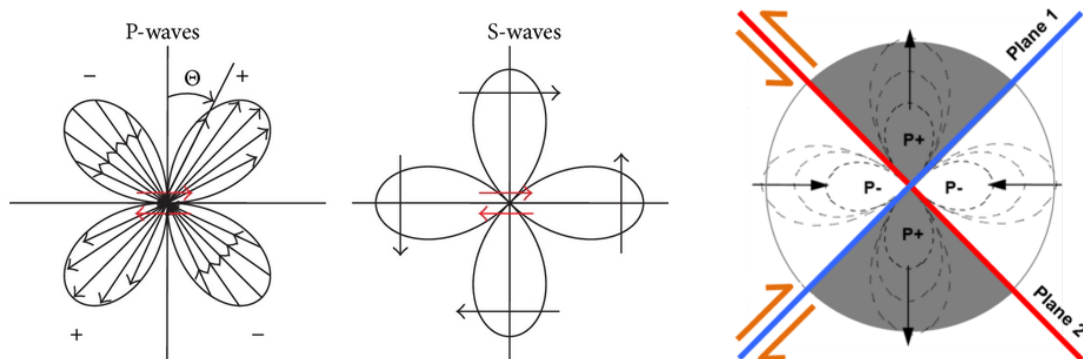

Fig. 2.15: P- and S-wave radiation pattern for a double-couple source in 2D and corresponding potential fault planes

Fig. 2.16 illustrates the displacement field produced by a slip on a crack (idealized earthquake source). In practise, fault plane solutions are constructed on the basis on a larger amount of earthquake registrations from stations located well distributed around the source (evaluation of positive and negative first signal onsets of P-waves).
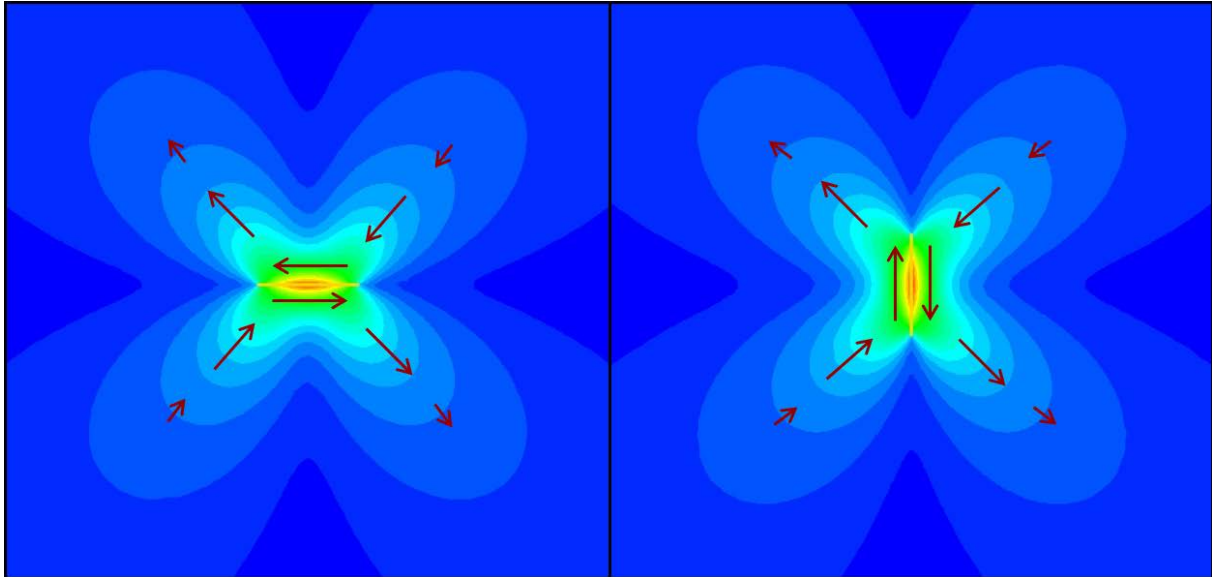

Fig. 2.16: Illustration of displacement field due to slip on a crack, arrows indicate displacement direction (mxrap, 2021)

2.5.2 Seismic moment, corner frequency and secondary source parameters

From the amplitude spectrum of P- and S-wave the long-period amplitude level A_0 and the corner frequency f_0 can be determined (see
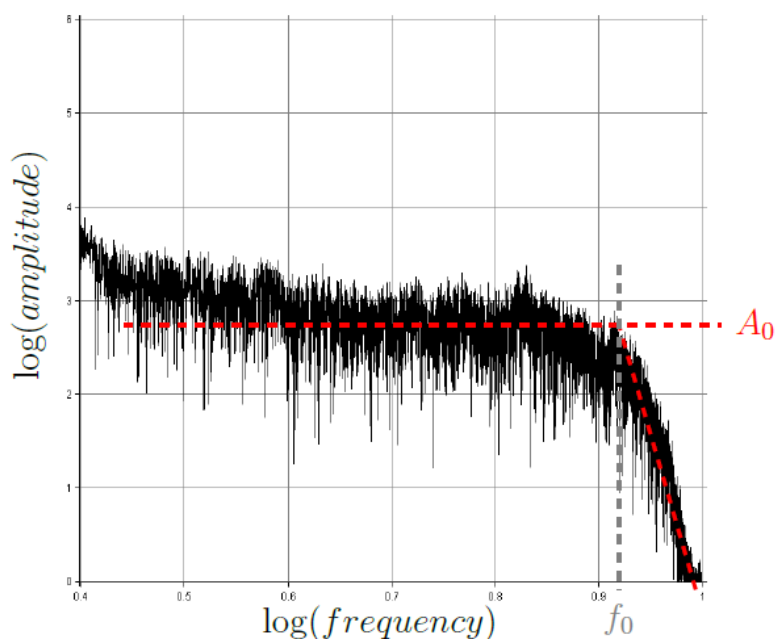Fig. 2.17).

Fig. 2.17: P-wave amplitude spectrum of an earthquake

The seismic moment M_0 is (like magnitude) a measure for the strength of the source process. From amplitude level the seismic moment is derived as follows.

$$M_0 = 4\pi\rho D_i v_p^{\,3} A_0 / \Phi \tag{2.19}$$

Φ represents the directivity factor (directional characteristic[1]) of the earthquake. The hypocentre distance to station i is denoted by D_i. The corner frequency f_0 characterizes the dimension of the seismic source. Assuming a circular source plane the source radius R is calculated from corner frequency after, for instance according to model of Madariaga 1976.

$$R = \frac{2v_p}{\left(2\pi f_0\right)^2} \tag{2.20}$$

The displacement D (slip at the source) can be calculated using shear modulus μ:

$$D = \frac{M_0}{\mu\pi R^2} \tag{2.21}$$

f_0, R, M_0 und M_w are closely linked.

Fig. 2.18 demonstrates these correlations graphically with the help of some global earthquakes.

[1] In case of a shear failure Φ can be obtained from fault plane solution.
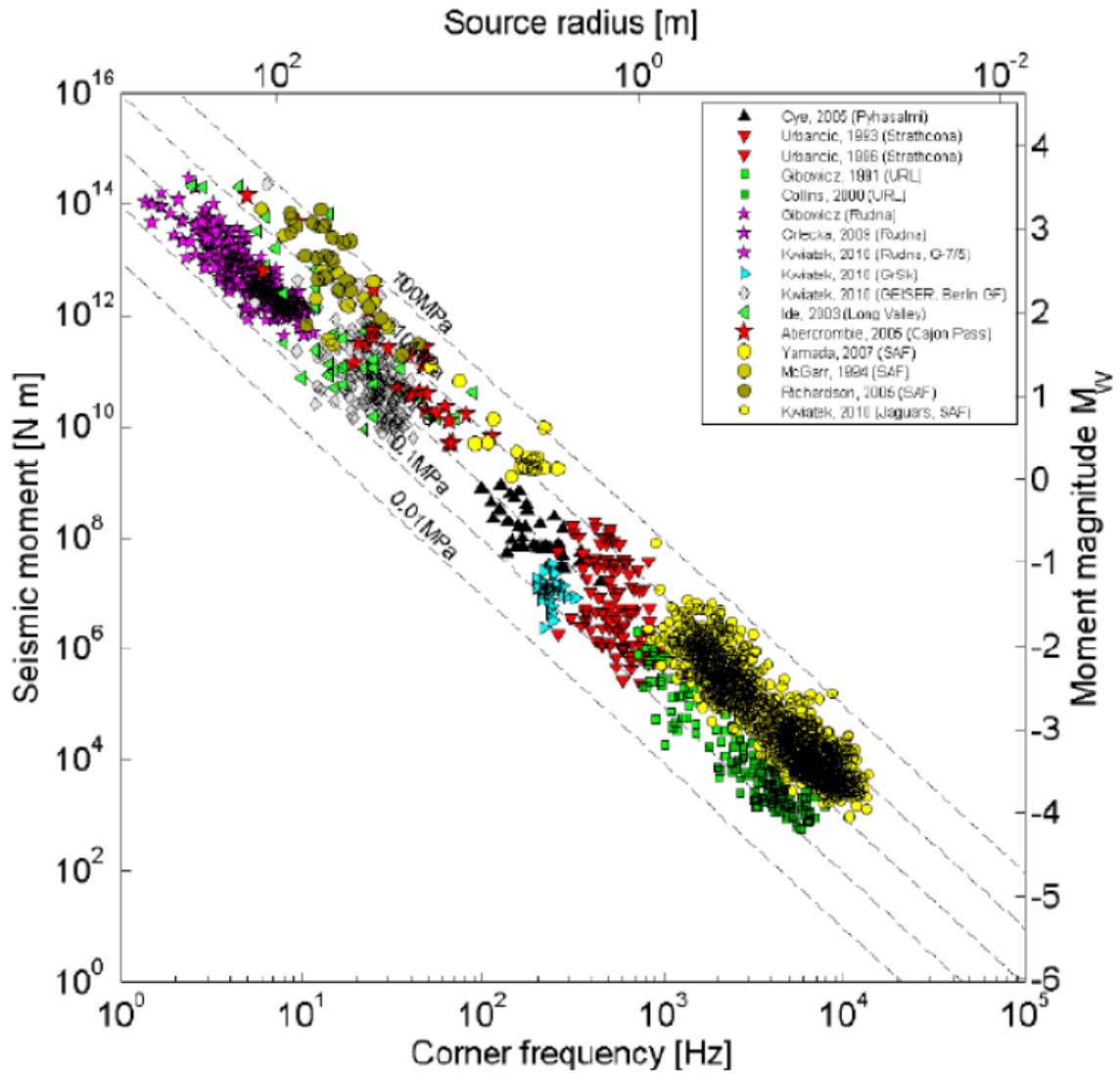
Fig. 2.18: Correlations between corner frequency, source radius, moment and magnitude of induced earthquakes (Kwiatek: presentation FKPE-Workshop 2010)

The difference between source stress σ_0 before and source stress σ_1 after the earth quake is called stress drop.

$$\Delta\sigma = \sigma_0 - \sigma_1 \tag{2.22}$$

Assuming a circular source, shear stress drop can be derived from displacement and source radius.

$$\Delta\sigma = \frac{7}{16} \cdot \frac{\pi\mu D}{R} \tag{2.23}$$

Stress drop is closely linked with the seismic moment M_{ij}. The seismic moment (tensor) is obtained by volume integration over moment tensor volume density m_{ij}.

$$M_{ij} = \iiint_V m_{ij}\,dV \tag{2.24}$$

The moment tensor volume density is a fictitious stress tensor, which is derived from the product of inelastic deformation tensor E_{ijkl} and the inelastic deformations ε_{ij}^T.

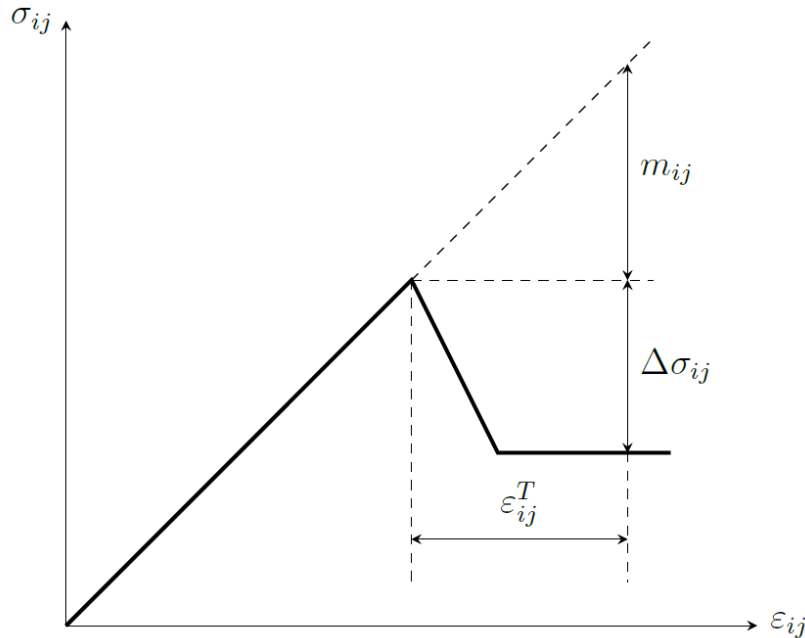$$m_{kl} = E_{ijkl} \cdot \varepsilon_{ij}^T \qquad (2.25)$$

Fig. 2.19: Visualization of seismic moment und stress drop

The seismic moment tensor is a symmetric tensor and can be decomposed on an orthogonal basis into 3 principal components (similar to the principal stresses of the stress tensor, see Fig. 2.20). According to the orientation of the principal components, the corresponding axis are defined as T (tension), N (neutral of intermediate) and P (pressure) axes. The principal components (eigenvalues) of M_{ij} are M_1, M_2 and M_3 with $M_1 > M_2 > M_3$.

The standard decomposition of the seismic moment tensor is based on three basic types of a source:

- Isotropic source (ISO)
- Double couple source (DC)
- Compensated linear vector dipole source (CLVD)

$$M_{ij} = M_{ij}^{ISO} + M_{ij}^{DC} + M_{ij}^{CLVD} \qquad (2.26)$$

A further decomposition into base tensors B_{ij} and coordinates M in the source-type space can be performed:

$$M_{ij} = M^{ISO} B_{ij}^{ISO} + M^{DC} B_{ij}^{DC} + M^{CLVD} B_{ij}^{CLVD} \qquad (2.27)$$

Dynamic events in rocks / rockmasses

Only for private and internal use!   Updated: 16 September 2021

The base tensors are as follows:

$$B_{ij}^{ISO} = \begin{bmatrix} 1 & 0 & 0 \\ 0 & 1 & 0 \\ 0 & 0 & 1 \end{bmatrix}$$ (2.28)

$$B_{ij}^{DC} = \begin{bmatrix} 1 & 0 & 0 \\ 0 & 0 & 0 \\ 0 & 0 & -1 \end{bmatrix}$$ (2.29)

$$B_{ij}^{CLVD+} = \frac{1}{2}\begin{bmatrix} 2 & 0 & 0 \\ 0 & -1 & 0 \\ 0 & 0 & -1 \end{bmatrix}$$ (2.30)

$$B_{ij}^{CLVD-} = \frac{1}{2}\begin{bmatrix} 1 & 0 & 0 \\ 0 & 1 & 0 \\ 0 & 0 & -2 \end{bmatrix}$$ (2.31)

Either B_{ij}^{CLVD+} or B_{ij}^{CLVD-} are used depending whether $M_1+M_3-2M_2 \geq 0$ or $M_1+M_3-2M_2 < 0$, respectively.

The magnitudes of the individual components are defined by following expressions:

$$M^{ISO} = \frac{1}{3}\left(M_1 + M_2 + M_3\right)$$ (2.32)

$$M^{DC} = \frac{1}{2}\left(M_1 - M_3 - \left|M_1 + M_3 - 2M_2\right|\right)$$ (2.33)

$$M^{CLVD} = \frac{2}{3}\left(M_1 + M_3 - 2M_2\right)$$ (2.34)

The scalar seismic moment M_0 describing the strength (magnitude) of the seismic event can be defined by the following expression:

$$M_0 = \left|M_{ISO}\right| + \left|M_{CLVD}\right| + M_{DC}$$ (2.35)

As mentioned already above: similar to the stress tensor, also the seismic moment tensor can be decomposed using eigenvalues and eigenvectors (λ_1, λ_2, λ_3) forming an orthogonal system. Fig. 2.21 and 2.22 show the most popular graphical presentations of the source type. Fig. 2.23 and 2.24 show in more detail the cubic and the bi-pyramid based presentations.

Fig. 2.23 shows the popular Hudson representation (cubic) of the seismic moment tensor. The classical double couple source (pure shear slip / shear cracking) is located at the centre (100% DC, no ISO component). Pure explosions and pure implosions are located at the top and bottom, with only either positive or negative ISO components. Fig. 2.24 shows the same in slightly different form (bi-pyramide presentation) indicating the ranges for pure tensile and pure compressive cracks as well as the strength of the DC component and the localization of the pure shear crack.

In case of a pure shear crack as seismic source (see Fig. 2.25) the scalar seismic moment can be determined by shear modulus G, slip area A and average slip (displacement) along the crack D:

$$M_0 = G \cdot A \cdot D \qquad \text{(see identical Equation 2.16)} \qquad (2.36)$$

Stress Tensor   **Moment Tensor**

$$\begin{bmatrix} \sigma_{11} & \tau_{12} & \tau_{13} \\ \tau_{21} & \sigma_{22} & \tau_{23} \\ \tau_{31} & \tau_{32} & \sigma_{33} \end{bmatrix} \qquad \begin{bmatrix} M_{11} & M_{12} & M_{13} \\ M_{21} & M_{22} & M_{23} \\ M_{31} & M_{32} & M_{33} \end{bmatrix}$$
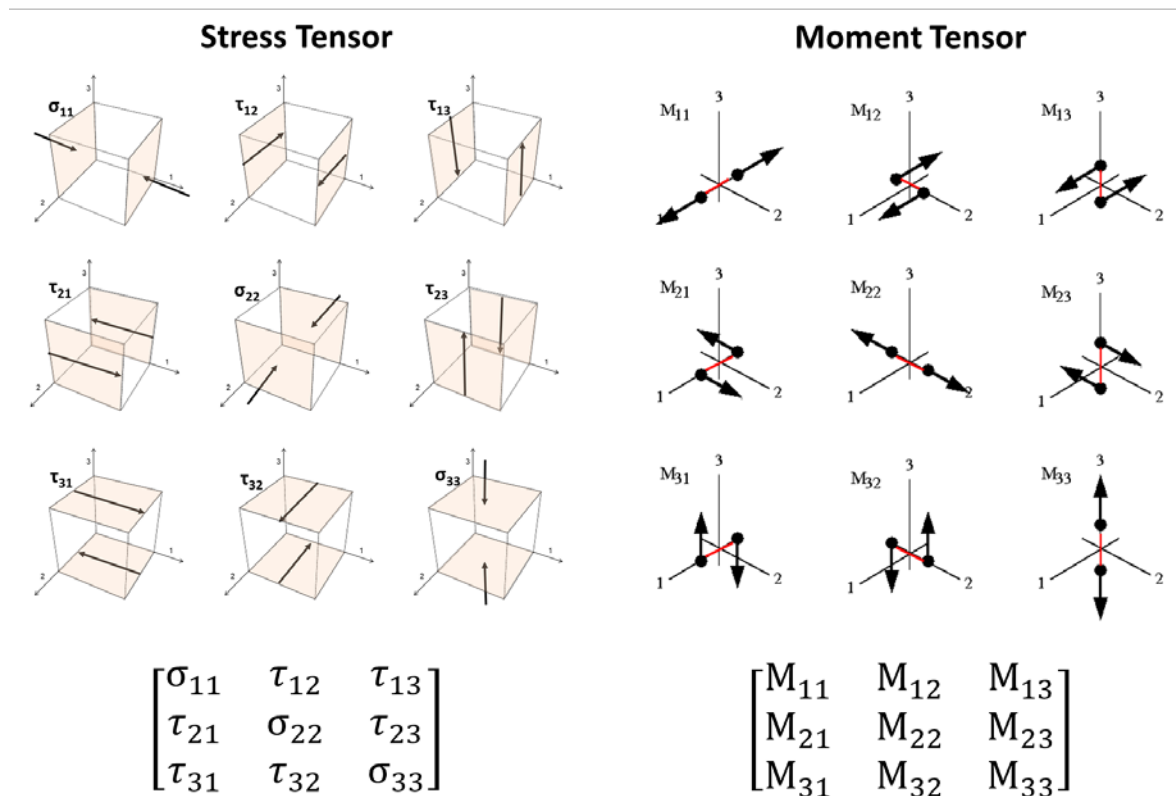
Fig. 2.20: Illustration of moment tensor in comparison to stress tensor (mxrap, 2021)

Dynamic events in rocks / rockmasses

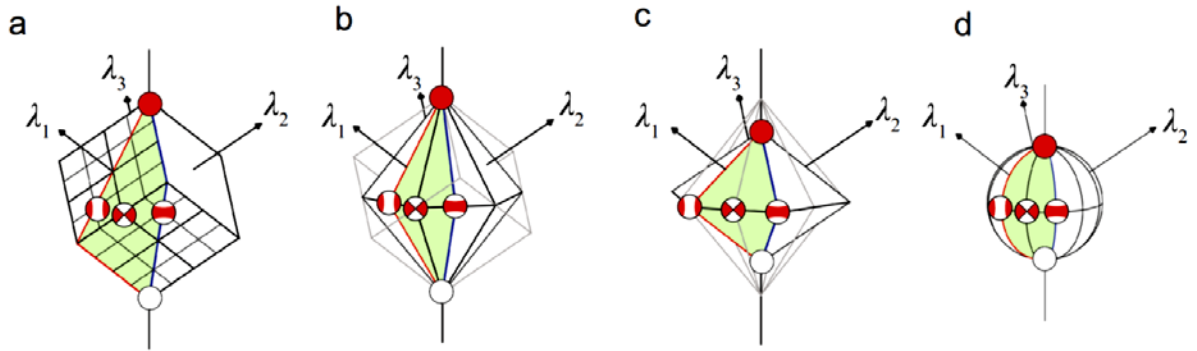Only for private and internal use!   Updated: 16 September 2021

Fig. 2.21: Moment tensor eigenvalue space and basal projections: a: basal cubic, b: basal hexagonal bi-pyramid, c: basal conjugate hexagonal bi-pyramid, d: basal spherical (Aso et al., 2016)
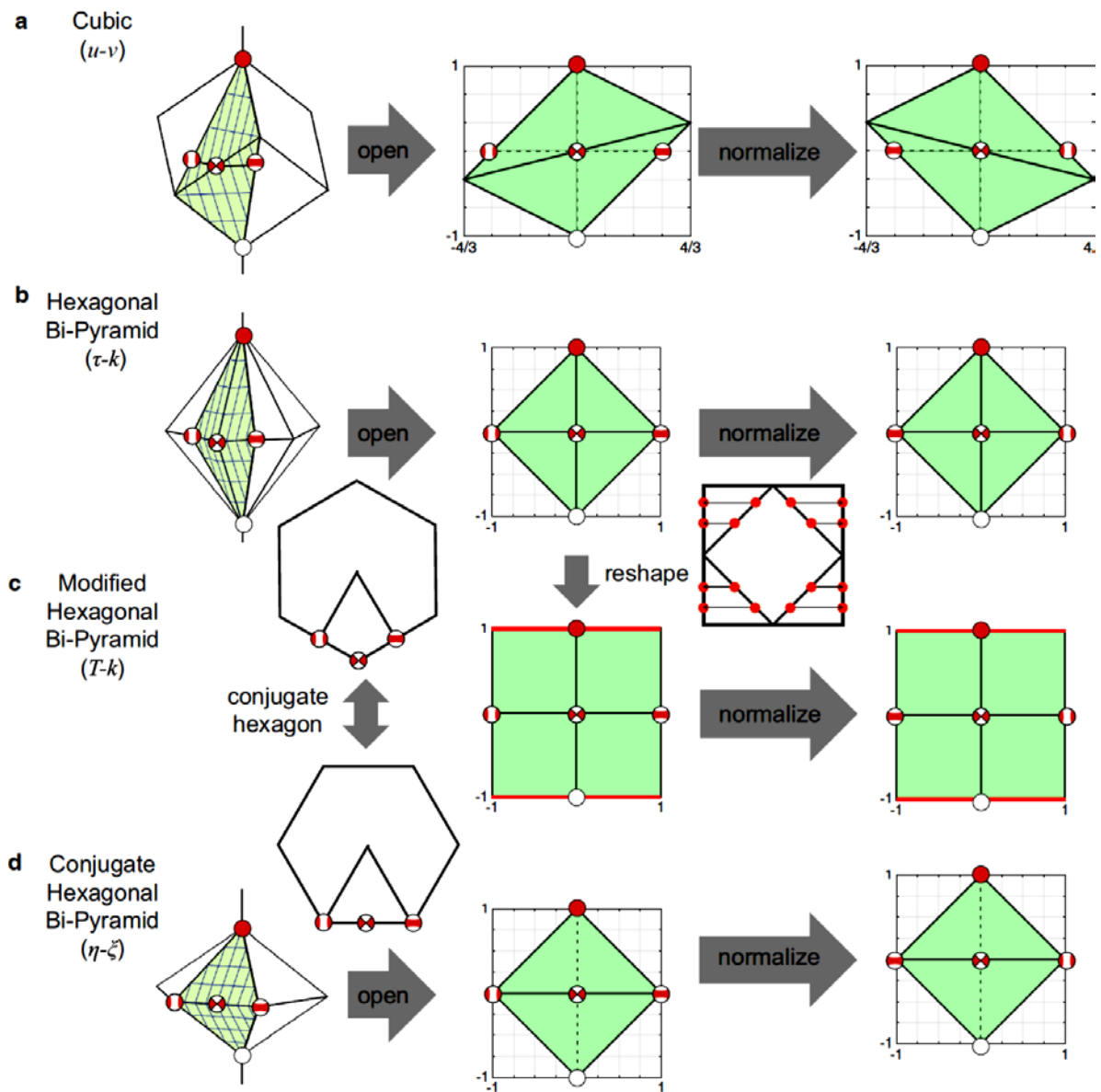

Fig. 2.22: 2D-Projections of source-type diagrams (Aso et al., 2016)

Dynamic events in rocks / rockmasses

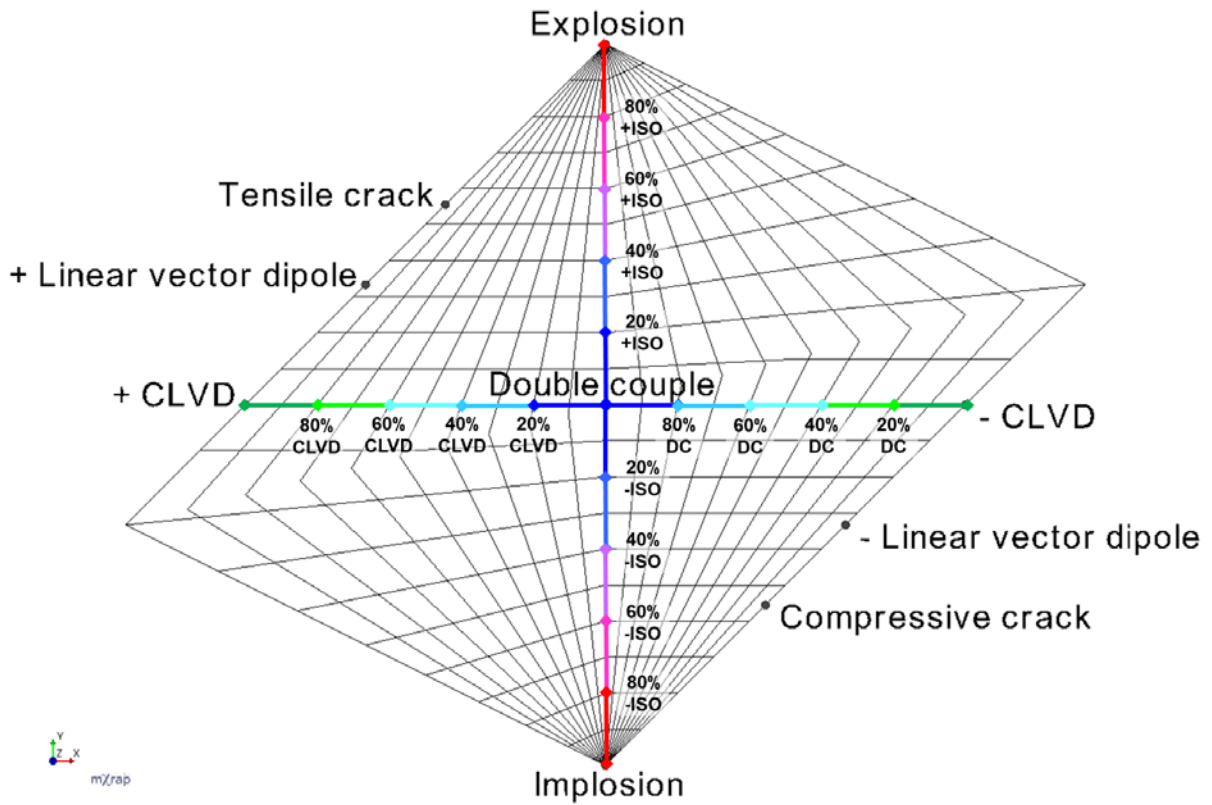Only for private and internal use!   Updated: 16 September 2021

Fig. 2.23: Hudson chart to visualize moment tensor decomposition (mxrap, 2021)
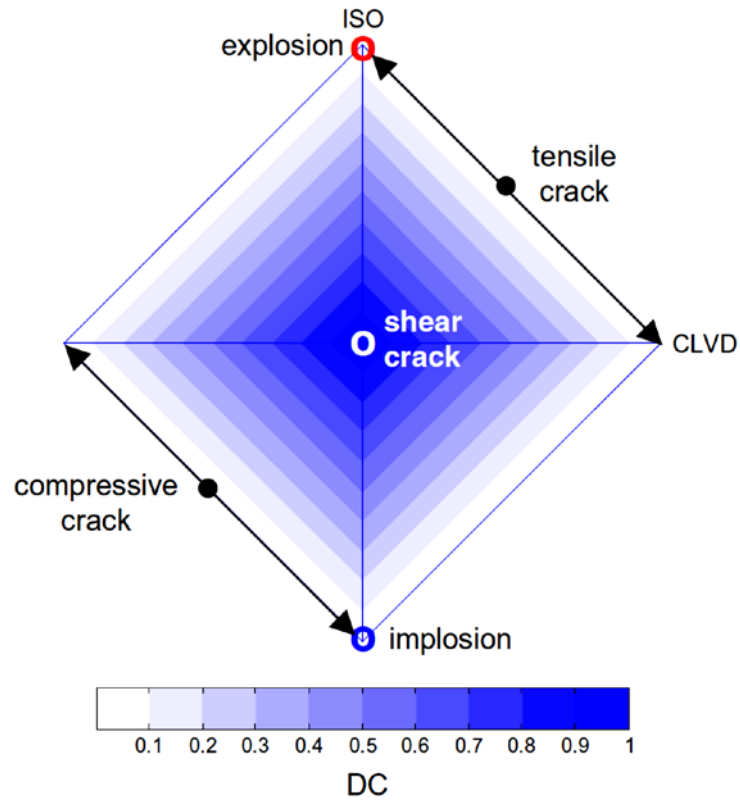
Fig. 2.24: Bi-pyramid chart to visualize moment tensor decomposition (Vavrycuk 2015)

Dynamic events in rocks / rockmasses

Only for private and internal use!   Updated: 16 September 2021
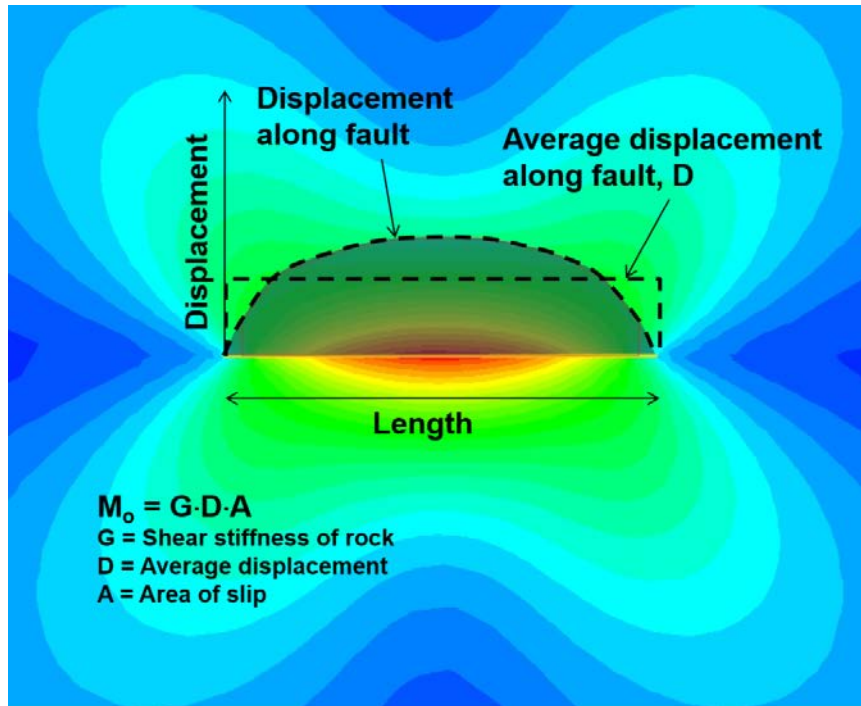
Fig. 2.25: Illustration of displacement field due to slip on a crack and main parameters to determine seismic moment (mxrap 2021)

The seismic moment tensor can be deduced by an inversion algorithm (see Fig. 2.26) considering the registered seismic signals and using Green's function, which describes the transmission of the waves from the source to the receiver (seismometer).

Fig. 2.26: Illustration of principle to deduce moment tensor by registration of seismic signals (mxrap 2021)

2.6 Sensors for seismic waves

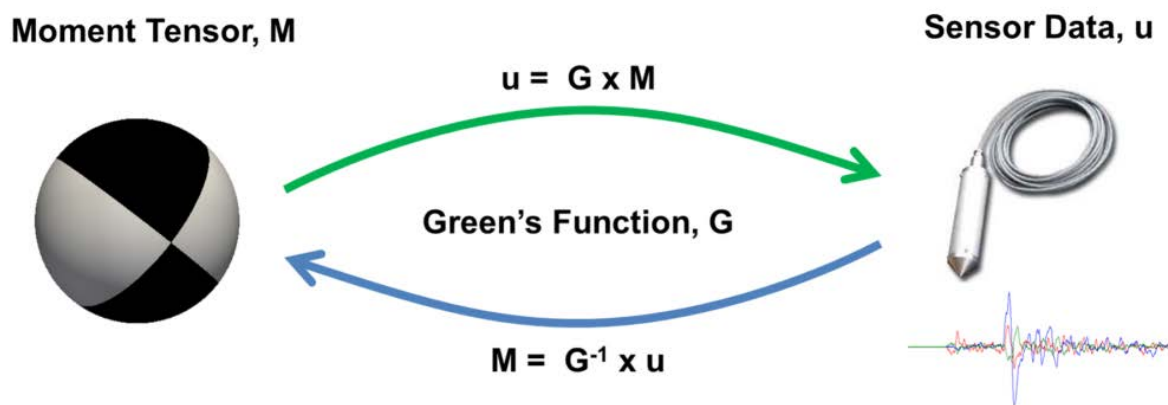We distinguish between deformation-proportional, velocity-proportional and acceleration-proportional sensors. In seismology mainly geophones and seismometers (technical advancement of seismographs) are established. These sensors convert mechanical vibrations acting at measuring point into a velocity-proportional electrical voltage. The voltage signal is amplified and digitized afterwards.

An inertia seismometer consists of a mass M, which is connected in parallel with a spring and a damper (see
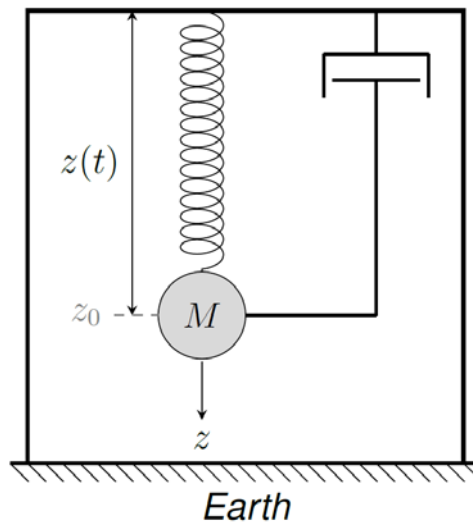Fig. 2.27).

Fig. 2.27: Inertia seismometer

Assuming that all movements are restricted in z-direction, then $u(t)$ is the movement of the earth and $z(t)$ is the relative movement of the mass M. In idle state the spring has a length of z_0. Two forces are acting on mass M in this system. The spring bears a force proportional to deflection z - z_0. With the stiffness of the spring k the force is obtained by - $k(z$ - $z_0)$. The damper bears a force proportional to its relative velocity $\dot{z}(t)$ between mass and earth. With damping constant C damping force is defined as $-C\dot{z}(t)$. With accelerations $\ddot{u}(t)$ and $\ddot{z}(t)$ following relationship is given.

$$M\big(\ddot{z}(t) + \ddot{u}(t)\big) = -C\dot{z}(t) - k\big(z(t) - z_0\big)$$
(2.37)

By setting $z_0 = 0$ the equation becomes

$$\ddot{z} + 2h\omega_0\dot{z} + \omega_0^2 z = -\ddot{u}$$
(2.38)

where $2h\omega_0$ = C/M and $\omega_0^2 = k/M$. Hence, acceleration $\ddot{u}$ can be described from a linear combination of $z(t)$ and its time derivations.

Seismographs are no longer used today. They were used before digital age and recorded soil movement by a needle on paper strips (see Fig. 2.28 left).

Geophones (see Fig. 2.28 middle) work the same way as inertia seismometers. They are used in seismic exploration, to gather information about the ground. There, usually artificial sources are used (hammer stroke, drop weight, vibratory plate or blast) to create seismic waves.

In modern seismometers (see Fig. 2.28 right) a magnet induces a voltage in a surrounding inductor. The measured voltage is amplified, digitized and either saved on site (offline station) or sent via internet connection to a data-collection centre (online station).
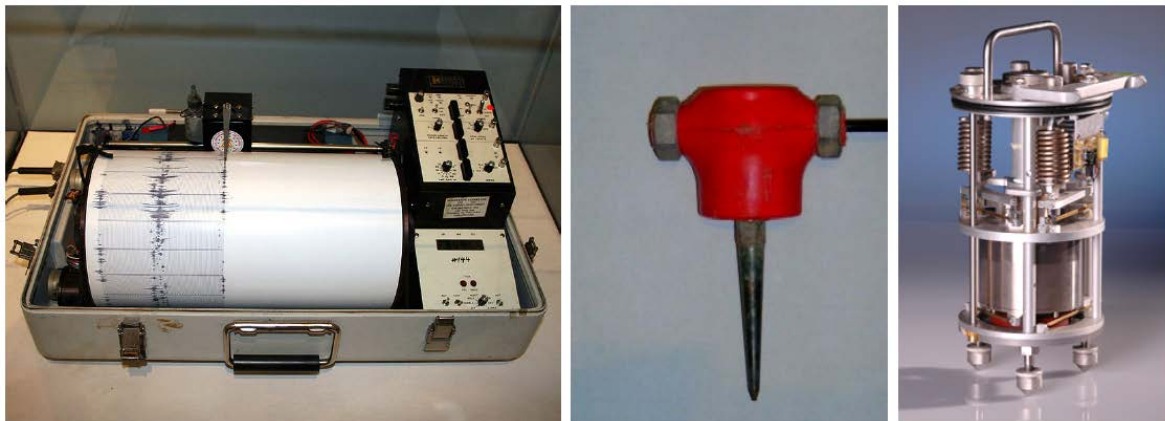

Fig. 2.26: Different seismic sensors: seismograph (left), geophone (middle) and inner life of a seismometer (right)

Both geophones and seismometers are available as 1-component variant (just vertical) and 3-component variant (1 vertical and 2 horizontal). They differ furthermore in their frequency sensitivity. For long-range seismic applications low-frequency sensors (0.01 - 10 Hz) and for microseismic applications high-frequency sensors (1 - 200 Hz) come to use.

2.7   Station networks

A requirement for a good source parameter determination is a good azimuthal coverage with stations around the epicenter region. In the ideal case stations are distributed with equal distance on a circle around the epicenter. For local earthquakes with magnitudes < 4 distances of several 100 meters to several kilometers are favourable. In this case the sensors should be desinged to record higher frequencies (seismometers with 1s- or 5s-pendular). For global events it is better to choose stations with higher distances. Here broadband seismometers (with 20s- or 100s-pendular) are favoured.
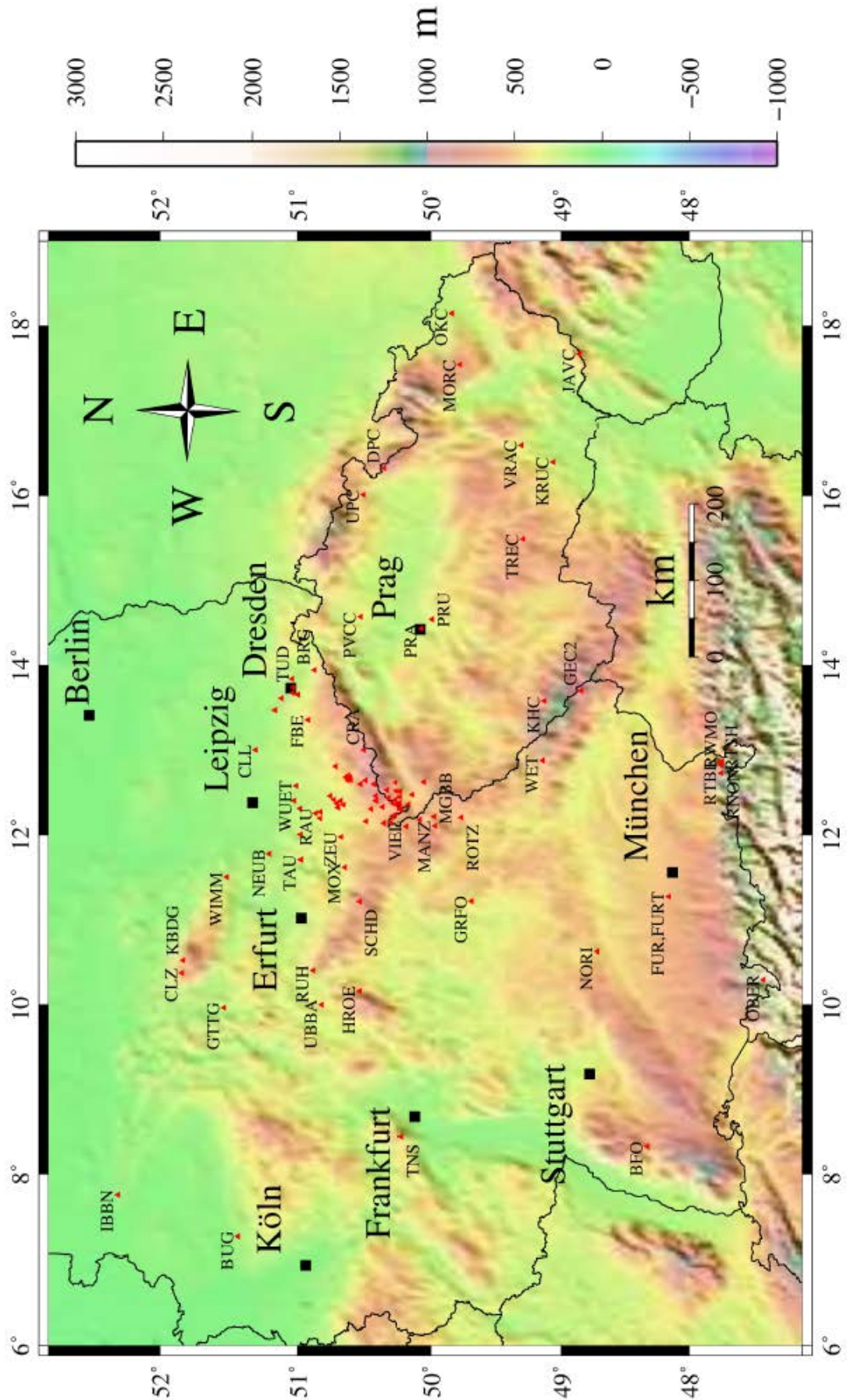
Dynamic events in rocks / rockmasses

Only for private and internal use!   Updated: 16 September 2021

Fig. 2.27: Distribution of seismological stations in central Germany and Czech Republic (Jakob, 2009)

3   Engineering seismology

Engineering seismology is understood as a branch of seismology, which provides required physical data about potentially destructive ground movements of earthquakes to the engineer who is responsible for earthquake-resistant constructions. In contrast earthquake engineering is an engineering discipline, which deals with design and construction of earthquake-resistant structures and thereto uses seismological output parameters provided by engineering seismology (Hurtig 1984).

3.1   Engineering seismological parameters

Every building represents a vibratory system, which responds different depending on its resonance on dynamic load caused by waves with corresponding frequencies. To translate the effect of an earthquake into engineering technically feasible parameters, spectral composition and polarization of seismic wave must be considered (Hurtig 1984).

Sensors (see section 2.6) can detect engineering seismological parameters ground acceleration a, ground velocity v and ground displacement s. But regardless of recorded physical parameters by the sensor, representation of adequate information of ground motion as acceleration, velocity or displacement is always possible, because:

$$s = \int v dt = \iint a dt^2 \text{ resp. } a = \frac{dv}{dt} = \frac{d^2 s}{dt^2} \tag{3.1}$$

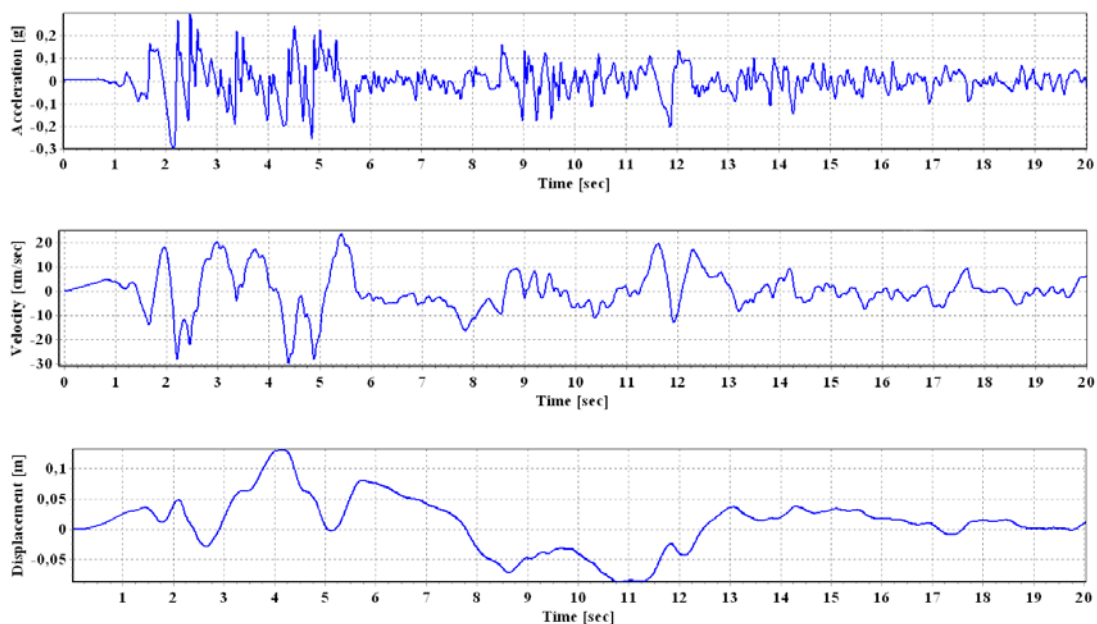Fig. 3.1 shows values for a, as well as calculated values for v and s for a typical earthquake.

Fig. 3.1: Acceleration recording of an earthquake plus calculated velocities and displacements

Dynamic events in rocks / rockmasses

Only for private and internal use!   Updated: 16 September 2021

Maximum values are denoted by a_{max} = PGA (Peak Ground Acceleration), v_{max} = PGV (Peak Ground Velocity) and s_{max} = PGD (Peak Ground Displacement). Dynamic stresses can be determined from velocities.

$$\sigma_{dyn}^{p} = \rho \cdot v_{p} \cdot v_c \quad \text{and} \quad \sigma_{dyn}^{s} = \rho \cdot v_{s} \cdot v_t \qquad (3.2)$$

v_c and v_t are corresponding vibration velocities.

When a seismic wave propagates through the earth, its frequency and amplitude changes (see section 2.1). Fig. 3.2 shows averaged response spectra [2] for an earthquake with 8 and 32 km source distance, respectively.
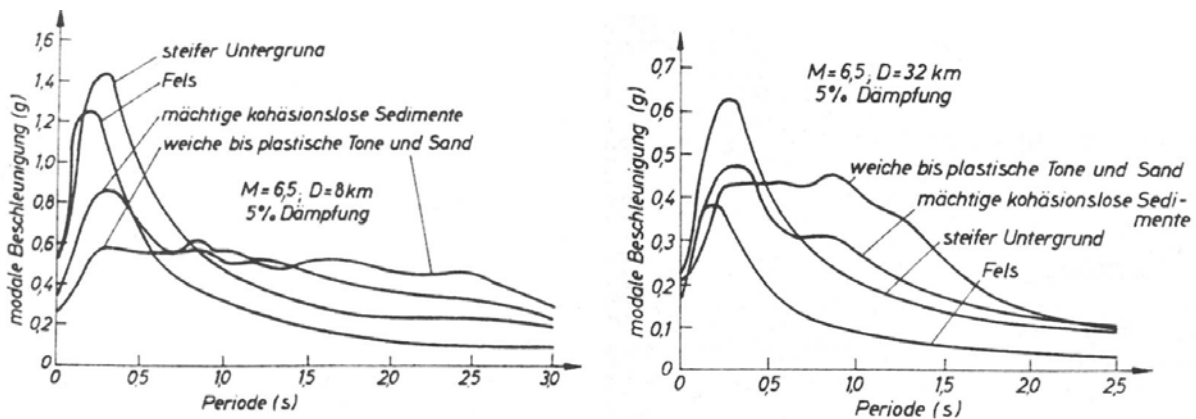

Fig. 3.2: Response spectra of horizontal accelerations of an earthquake with magnitude 6,5 in 8 km (left) and 32 km (right) source distance (after Seed et al. 1974 in Hurtig 1984)

The curves in Fig. 3.2 show, that big amplitudes with higher frequencies (T = 1/f < 0.5 s) occur in small distance (8 km). With increasing source distance the influence of damping becomes apparent. At soft underground damping effect is compensated due to soil reinforcement within a certain period range, so that a relative delay of amplitudes is observed compared to amplitudes on rocky underground. In a period range of 0.5 to 1.5 s and source distance of 32 km it becomes apparent, that amplitudes are higher at soft underground (Hurtig 1984).

3.2   Estimation of maximal magnitude

For every region maximal magnitude M_{max} and intensity I_{max} exist. Their determination is extremely important for assessment of earthquake hazard. However, there are only few reliable approximate approaches (Hurtig 1984). Two of them are presented in the following subsections.

---

[2] Response spectrum is achieved by Fourier transformation of time series (e.g. accelerations) into the frequency domain.

3.2.1 Magnitude-frequency relation

The Gutenberg-Richter law describes the relation between magnitude and occurrence frequency of earthquakes in a considered area.

$$\log_{10} N = a - bM \tag{3.3}$$

Where N is the number of earthquakes, that have a magnitude of $\geq M$. a and b are constants, whereupon b generally[3] is near 1. Fig. 3.3 shows the Gutenberg-Richter relation for micro-earthquakes in the area Schlema/Alberoda (Germany). In the time span between 1998 and 2013 approx. 1650 events were registered in this area.
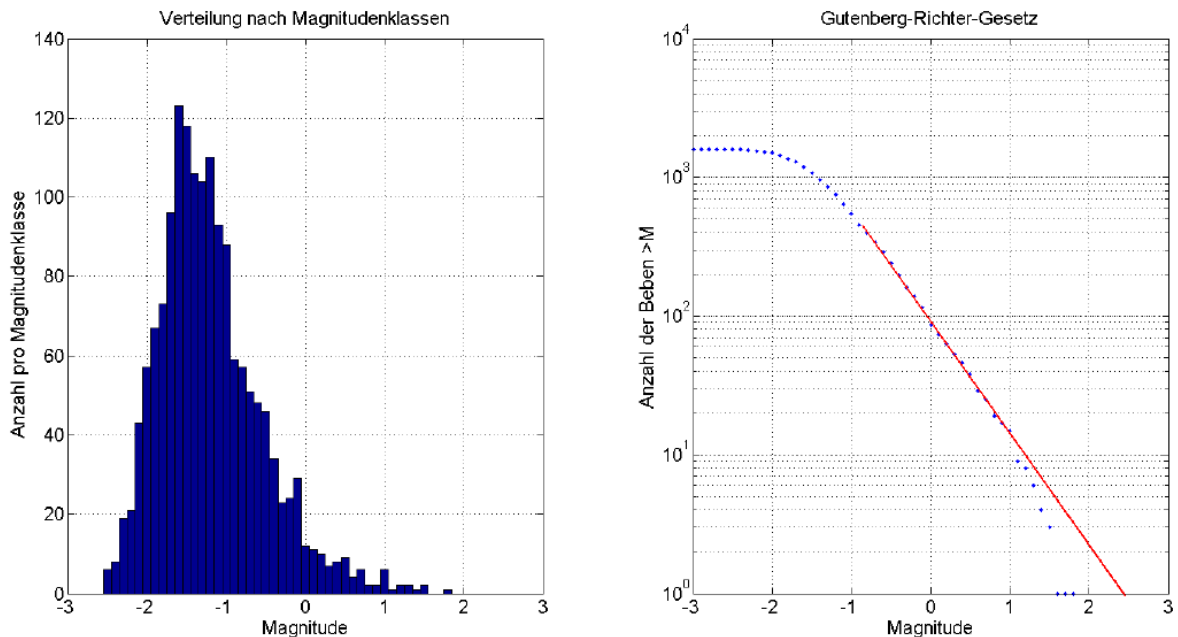
Fig. 3.3: Gutenberg-Richter relation for the area Schlema/Alberoda (Schütz & Konietzky, 2016)

Smaller events are harder to detect by seismic sensors, because their amplitudes are near the noise level. For this reason the maximum number of events is at a magnitude of − 1.5 (see Fig. 3.3). At higher magnitudes the relation usually bends down because observation time is too small for statistical analysis of big earthquakes. By installing a straight line at the linear part of the relation (red line in Fig. 3.3) maximum magnitude can be estimated (here: $M_{max} \approx 2.5$). Hurtig 1984 proposes for estimation of M_{max} and I_{max}:

$$M_{max} = M_{max,beobachtet} + 0.5 \text{ resp. } I_{max} = I_{max,beobachtet} + 1 \tag{3.4}$$

---

[3] The b-value describes the ratio of small to big earthquakes. For example: if many small and few big earthquakes occur, b-value is > 1.

Dynamic events in rocks / rockmasses

Only for private and internal use!   Updated: 16 September 2021

3.2.2 Benioff curve

The Benioff curve represents the cumulative release of energy within an area with time t (Hurtig 1984).

$$\sum \sqrt{E_i} = f(t) \tag{3.5}$$

Where E_i is the release of energy for a single earthquake.
Fig. 3.4 shows the Benioff curve of eastern Germany since 1500. The curve shows clearly periods of weak and strong activity (Grünthal 1981).

From this curve some conclusions can be derived: Assuming that total activity of the region of interest is limited by an upper and a lower strain state (dashed lines in Fig. 3.4), a possible maximal earthquake can be defined as abrupt release of energy from lowest to peak state. This would give a maximal magnitude of 5.7 for the investigated territory (Grünthal 1981).
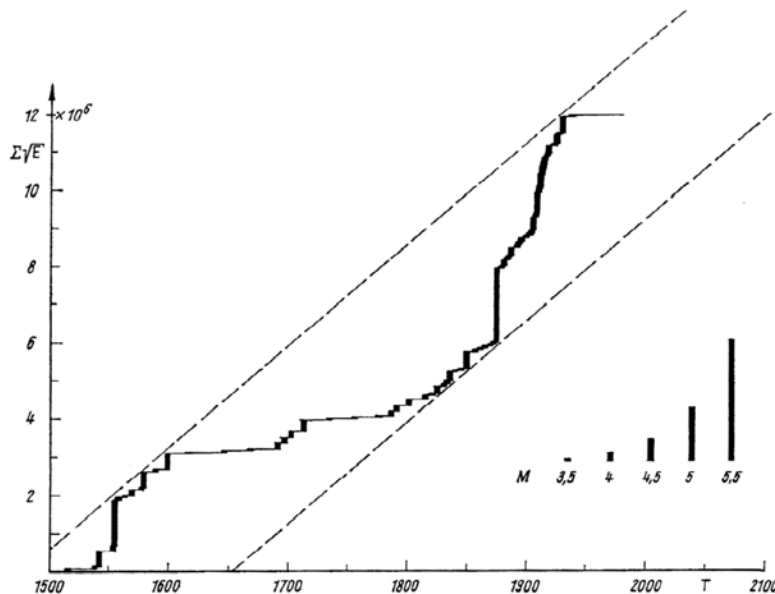
Fig. 3.4: Benioff curve for the territory of the GDR since 1500 with energy E in Joule (Grünthal, 1981)

3.3 Estimation of peak ground velocities

From the empirical relation

$$PGV_0 = k_1 \cdot M_{max} + k_2 \tag{3.6}$$

hypocentre peak ground velocity PGV_0 can be estimated. k_1 and k_2 are empirical coefficients, that have to be determined from a given data set for the specific investigation area. Peak ground velocity PGV (x) changes with distance x according to the following relationship:

$$PGV(x) = PGV_0 \cdot e^{-\alpha_t x} \tag{3.7}$$

Here α_t is a theoretical damping parameter that contains energy dissipation resulting from diffusion and damping. α_t is obtained by the seismic quality factor Q, that depends on frequency f and phase velocity c of the seismic wave.

$$Q = \frac{\pi f}{\alpha_t c}$$ (3.8)

Near the source geometrical spreading dominates. This can be considered in equation (3.7) by multiplication by factor 1m/x(m).

Fig. 3.5 shows the decrease of peak ground velocities with distance x for different magnitudes for the region Schlema/Alberoda.
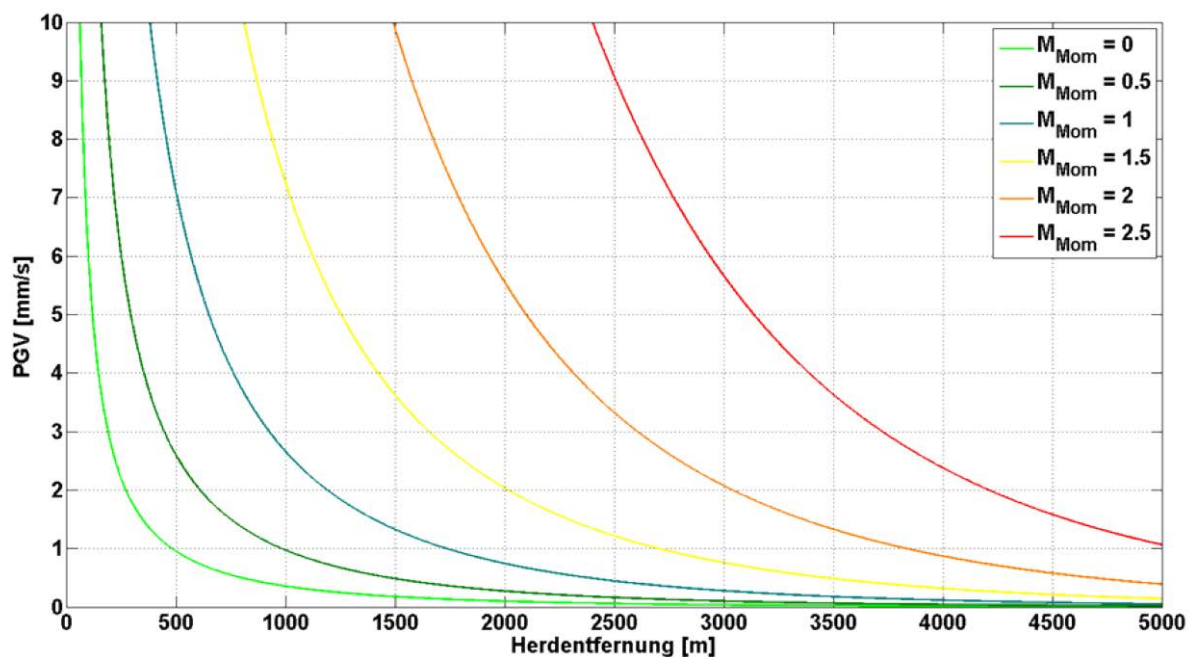
Fig. 3.5: Peak ground velocities for different magnitudes and source distances (Schütz & Konietzky, 2016)

3.4   Legal standards

For the construction of buildings in seismic areas special regulations apply. The aim is to save human life, to limit damage and to ensure, that important constructions for public safety and infrastructure stay operable in the case of an earthquake. Following standards are defined by the legislator:

The European standard Eurocode 8 (EN 1998) "Design of structures for earthquake resistance" applies for design and construction of buildings and structures in seismic areas. It contains regulations for ordinary as well as special constructions e.g. nuclear facilities, big dams or offshore-constructions.

The DIN 4149 (2005-04) "Bauten in deutschen Erdbebengebieten" applies for conceptual and structural design and construction of usual buildings.

Essentially the force F acting on a building or part of the building is calculated. Newton's second law says, that the force F is given by multiplication of mass m (here: building mass) and the acting acceleration a (here: rated ground acceleration a_g). Different factors affect applied force F. Hence the law is extended by a function f to consider these factors.

$$F = m \cdot a_g \cdot f\left(factors\right) \tag{3.9}$$

According to DIN 4149 Germany is subdivided into earthquake zones 1 to 3 (see Fig. 3.6). Seismic risk outside of zones 1 to 3 is regarded as so low, that special consideration of earthquake impact is not necessary.
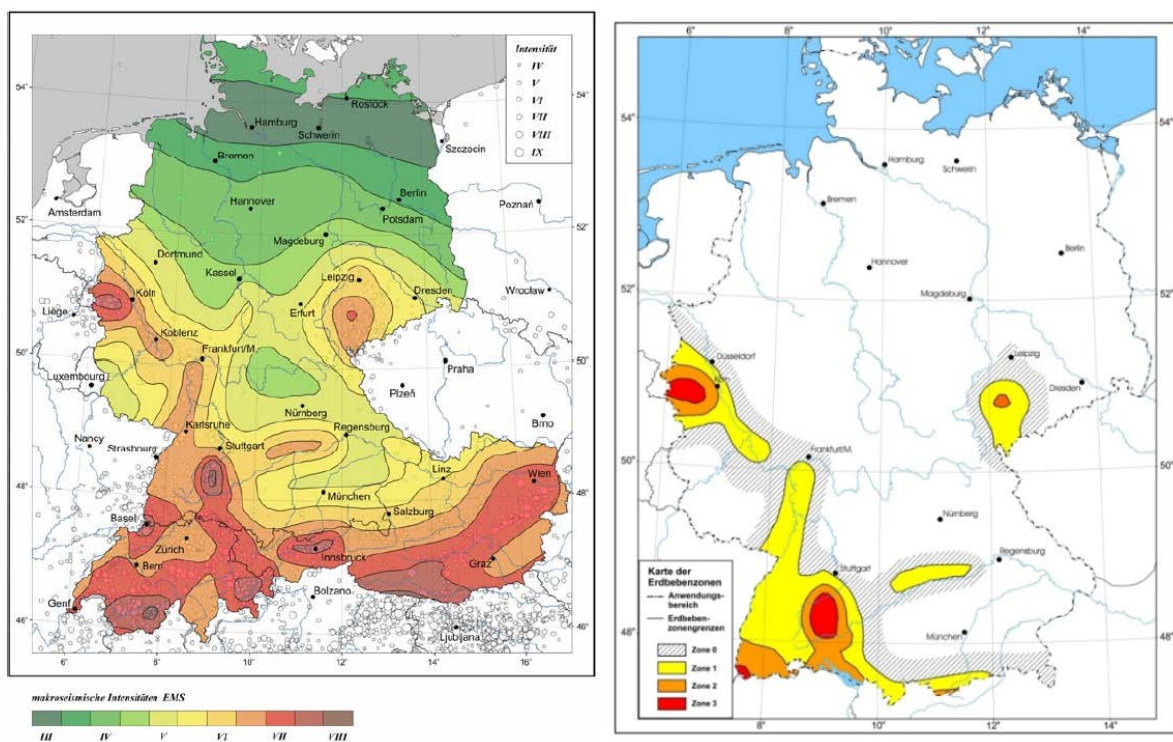
Fig. 3.6: Maps: Earthquake intensity (left) and earthquake zones (right) in Germany (source: Grünthal 2004 and DIN 4149)

In DIN 4149 rated ground acceleration a_g is applied as zone specific parameter.

Tab. 3.1: Rated ground acceleration relating to earthquake zones and intensity range

earthquake zone	intensity range	a_g in m/s^2
1	$6.5 \leq I < 7$	0.4
2	$7 \leq I < 7.5$	0.6
3	$7.5 \leq I$	0.8

Dynamic events in rocks / rockmasses

Only for private and internal use! Updated: 16 September 2021

Factors are:
- Regularity of the construction → behaviour factor
- Geological bedrock → control periods of response spectrum and bedrock parameters
- Importance of the construction → importance factor
- Construction damping → damping correction factor
- Correction factor for multi-story buildings

A method for determination and assessment of impact on buildings caused by vibrations is defined in DIN 4150-3 (1999-02) "Erschütterungen im Bauwesen". The assessment is based on guide values for velocities of short-time and long-lasting vibrations (see Tab. 3.2 and Tab. 3.3).

Tab. 3.2: Guide values for velocities for assessment of impact of short-time vibrations on buildings (source: DIN 4150-3)

Type of building	Guide values for velocities v_i in mm/s Base frequencies		
	1 Hz to 10 Hz	10 Hz to 50 Hz	50 Hz to 100 Hz
Commercially used buildings, industrial and similar buildings	20	20 to 40	40 to 50
Residential buildings and constructions with similar usage	5	5 to 15	15 to 20
Buildings with special shock sensitivity not matching with the above ones and especially worth preserving	3	3 to 8	8 to 10

Tab. 3.3: Guide values for velocities for assessment of impact of long-lasting vibrations on buildings (source: DIN 4150-3)

Type of building	Guide values for velocities v_i in mm/s Uppest ceiling, horizontal, all frequenzies
Commercially used buildings, industrial and similar buildings	10
Residential buildings and construction with similar usage	5
Buildings with special shock sensitivity not matching with the above ones and especially worth preserving	2.5

The estimation of peak ground velocities is described in section 3.3. The received values for PGV are compared with the guide values.

4   Induced seismicity

Engineering activity of humans can strongly influence the stress state near the surface, so that earthquake-like events called induced seismicity can be generated. Even in mainly aseismic areas strong earthquakes can be caused in this way (Hurtig 1984).

4.1   Surface dam induced seismicity

Earthquakes are denoted as dam induced, when significant space and time relationships with dam parameters and storage regime are observable. The occurrence of seismic events during construction and operation of surface dams may constitute a serious danger for the dam itself and also for residential areas downstream of the dam. Generally seismicity increases at filling the dam, but there are also references on decreasing seismicity especially in seismic active areas (Hurtig 1984).

The maximal observed magnitude of a dam induced event was approx. 6.3 at December, 10, 1967 in India (Koyna dam). Because of this event around 200 humans lost their life, over 1500 were hurt and thousands got homeless. The dam got damaged, but resists.

Significant dam induced changes in seismicity were detected at over seventy sites worldwide. Among all the factors, storage regime most likely correlates with the observed induced seismicity (Gupta 1992). It is proven, that dam induced events occur mainly in areas, where the earth's crust is heterogeneous near the surface and under significant latent tectonic stresses. Fault plane solutions obtained so far show nearly exclusively either normal slip or horizontal displacements. It is noteworthy, that movement process and fracture direction, obtained by fault plane solutions, correlate with the tectonic deformation regime and the orientation of main stress axes. Thus the mechanism of induced seismic events can be explained with given tectonic settings (Hurtig 1984).

According to Hurtig (1984) there are two interpretation models for explanation of dam induced seismicity. The load model sees additional stresses, generated by load of the accumulated water interfering with the present tectonic stresses, as cause of the events. Thus stress increase can reach (at water filling of 100 m) maximal 10 bar. The pore fluid model assumes a reduction of effective stresses by increasing pore water pressure. The effect of an increased pore pressure leads to a shift of the MOHRs circle at constant radius to the left (see
Fig. 4.1). When reaching MOHRs failure envelope failure can occur. Simultaneously, water infiltration can lead to a decrease of the friction coefficient (Hurtig 1984).
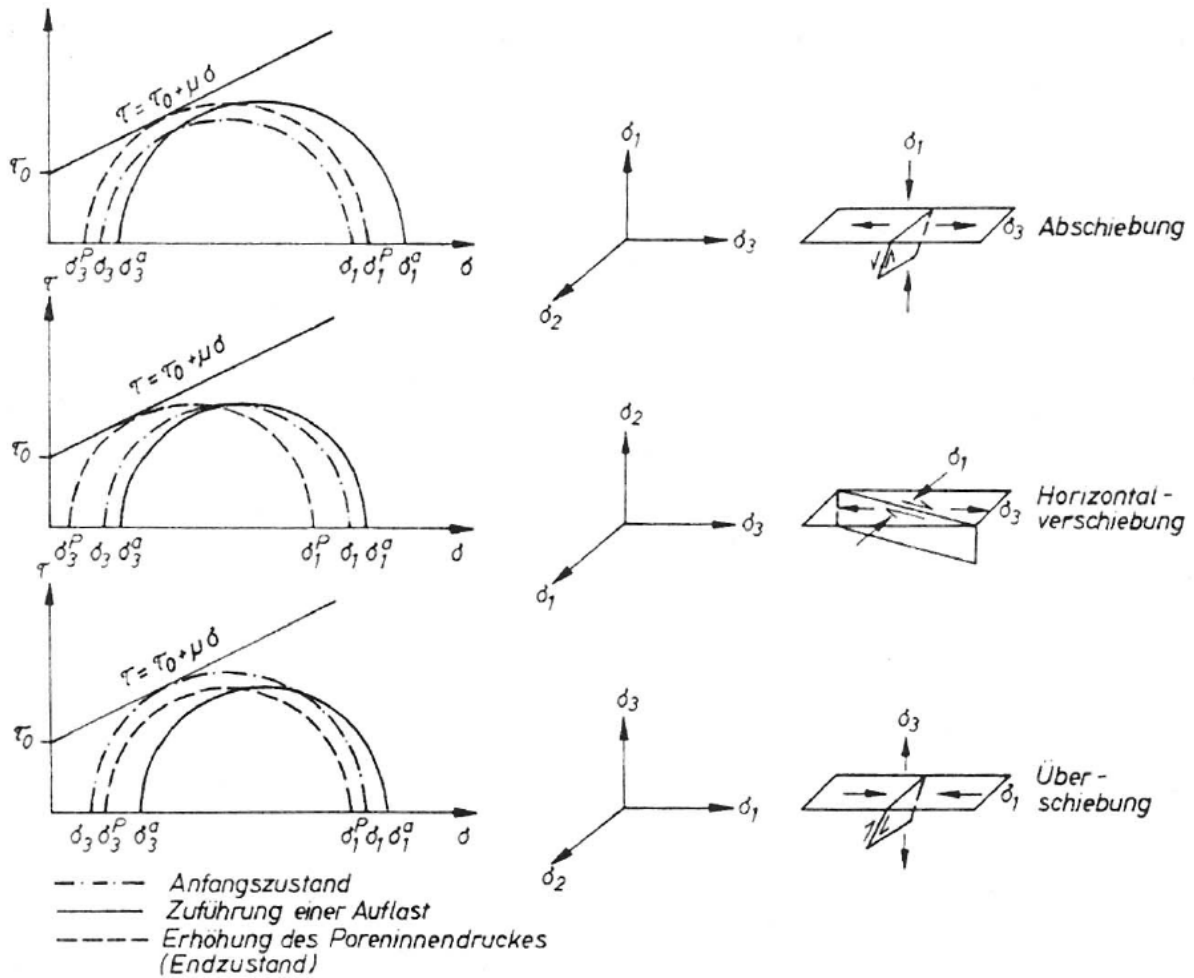
Fig. 4.1: Influence of load (a) and changes in pore pressure (P) on stress field (according to Simpson 1976: Hurtig 1984)

4.2 Mining induced seismicity

In numerous mining areas in the world seismic events are detected related to underground mining activities. Very often mining induced seismic events are observed in coal mining regions. Strong seismic activity is also known from ore and salt mining areas (Hurtig 1984).

Because of the variety of complex relationships (geomechanical causes, prerequisit and promoting factors) a classification of mining induced events is still not clearly possible. Hurtig (1984) speaks therefore in general of "seismic events in mining areas" and divides into these three types:

- ▪ indirect Earthquakes in mining areas[4] causing damage at constructions on and below the surface or trigger seismic events in the extraction area.

- ▪ Type I: The local mining induced stress field triggers seismic events in the extraction area. This type corresponds largely to the existing conception of rock bursts. Hurtig (1984) denotes this type as extraction induced seismicity.

- ▪ Type II: Underground cavities causes long-range stress rearrangements in a long-term, that can cause earthquakes. Hurtig (1984) denotes this type as digging induced seismicity. Thereby the events are in no relationship with the current extraction operation.

However above mentioned classification comprises only the failure of underground mine workings. Further events, covered by the term mining induced seismicity, are:

- • Seismicity in opencasts (mass rearrangements with and without soil liquefaction)
- • Events triggered by drilling (specifically at natural gas/raw oil extraction)
- • Injection induced seismicity (geothermal energy, fracking, see also section 4.3)
- • Fluid extraction induced seismicity (geothermal energy, natural gas/raw oil)
- • Blast induced seismicity
- • Events triggered by influx (dissolution in salt or karst)

In Germany the strongest events occurred in salt mining (see Tab. 4.1).

Tab. 4.1: Induced seismic events in German mining areas with M_L > 4.0 or I > 6 (Grünthal & Minkley 2005)

Date			Location	M_L	I_0
Year	Month	Day			
1888	3	18	Ruhrgebiet NW	3.6	VI
1936	11	3	Ruhrgebiet NW	3.9	VI - VII
1940	5	24	Krügershall, Saale-Revier	4.9	VII
1943	3	5	Schierstedt, Nord-Harz	3.9	VI - VII
1953	2	22	Heringen, Werra-Revier	5	VII - VIII
1958	7	8	Merkers, Werra-Revier	4.7	VII
1961	6	29	Merkers, Werra-Revier	3.6	VI
1971	4	4	Aschersleben, Nord-Harz	3.9	VI - VII
1975	6	23	Sünna, Werra-Revier	5.2	VIII
1981	7	13	Ibbenbüren	4.1	VI
1989	3	13	Völkershausen, Werra-Revier	5.6	VIII - IX
1991	5	16	Ibbenbüren	4.3	VI
1996	9	11	Teuschenthal, Saale-Revier	4.9	VII
2003	1	6	Ibbenbüren	4.2	VI

---

[4] Mostly a natural earthquake is assumed as cause. But it usually cannot be excluded, that these earthquakes were triggered itself by mining activities !

Dynamic events in rocks / rockmasses

Only for private and internal use!   Updated: 16 September 2021

4.3   Injection induced seismicity

By grout injecting of liquids in deep boreholes earthquakes can be induced. During hydraulic fracturing this is even desired, because the generation of cracks is desired to create or extend flow paths. In particular this procedure is used for extraction of raw oil and natural gas as well as at hydraulic salt production (leaching) and in deep geothermal systems. Thereby pre-existing fault zones can be reactivated (see Fig. 4.2) or unfractured rock will be stimulated by crack formation (Hot-Dry-Rock-Method).
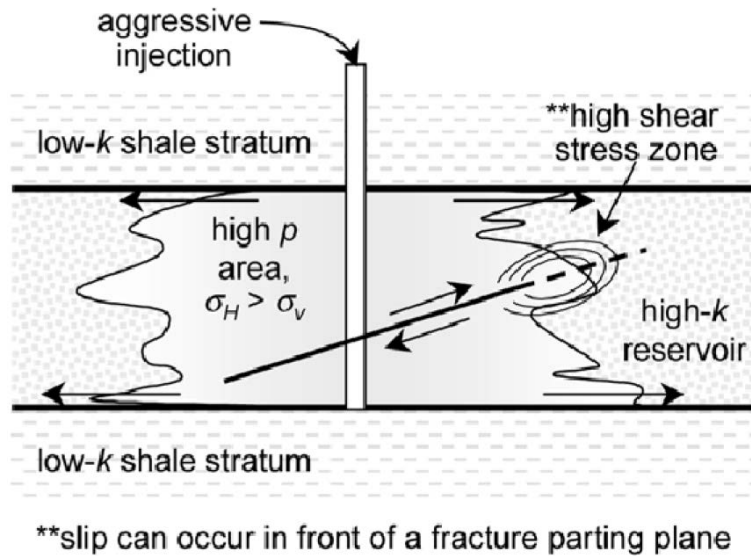

Fig. 4.2: Schematic illustration of a reactivated fault zone at fracking (Dusseault et al. 2001)

Similar to surface dam induced events (see section 4.1) the increasing pore pressure reduces the effective stresses (see Fig. 4.1).

Some examples of injection induced events in Europe are shown in the following table. Interestingly no relationship between maximal magnitude and peak ground acceleration (PGA) can be inferred from this table.

Tab. 4.2: Selected events of injection induced seismicity with maximal magnitudes (Evans et al. 2012)

Location/Country	Depth [km]	Rock	PGA [% g]	Date	Type	p_w^{max} [MPa]	$V_{inj.}$ [m³]	M_L^{max}
Soultz/FR	3.5	Granite	8	1993	Stimulation	10	20·10³	1.9
Soultz/FR	5.0	Granite	8	2003	Stimulation	18	37·10³	2.9
Bad Urach/DE	4.3	Gneiss	9	2002	Stimulation	34	5.6·10³	1.8
KTB/DE	9.0	Gneiss	6	1994	Inject. test	55	200	1.2
Landau/DE	3.0	complex	8	2007	Circulation	6.0	Balanced	2.7
Hellisheidi/IS	2.5	Basalt	49	2003	Drill&Stim.	1.7		2.4
Monte Amiata/IT	3.0	Metam.	19	1969	Circulation			3.5
Basel/CH	5.0	Granite	15	2006	Stimulation	30	12·10³	3.4
Unterhaching/DE	3.6/3.35	Carb.	5	2007	Circulation	2.5	Balanced	2.4
Larderello/IT	2.0	Carb.	16	1977	Circulation			3.0
Latera/IT	1.0	Carb.	19	1984	Injection		Balanced	2.9
Torre Amiata/IT	2.0	Carb.	20	1977	Injection	1.2	4.2·10³	3.0
Cesano/IT	2.0	Carb.	14	1978	Injection	7.5	2·10³	2.0

Based on the example Basel, this processes is explained in more detail. The Basel-1 borehole was put down between May and October 2006 to a depth of 5 km. In this depth granitic rocks reach a temperature of 200°C in this region, which makes a geothermal use economical interesting. The stimulation (fracking), performed in December 2006, induced a notable seismic activity. In consequence the project had to be aborted and a complete seismic risk analysis took place (Delacou and Sartori 2009). As part of the stimulation, 11500 m^3 water were injected under high pressures. The injection rate reaches temporary 3300 l/min, which leads to a maximum wellhead pressure of nearly 300 bar (see
Fig. 4.3). A network of seismometers installed around the borehole detected 10.500 seismic events during the stimulation. The seismic activity reached its maximum as expected at maximal injection rate. Although the pressure after closing the borehole (shut-in) already dropped sharply, the biggest detected event reached a magnitude M_L = 3.4 and intensities of IV to V (EMS-98). Further three aftershocks with M_L > 3 occurred in January and February 2007 (Delacou and Sartori 2009).
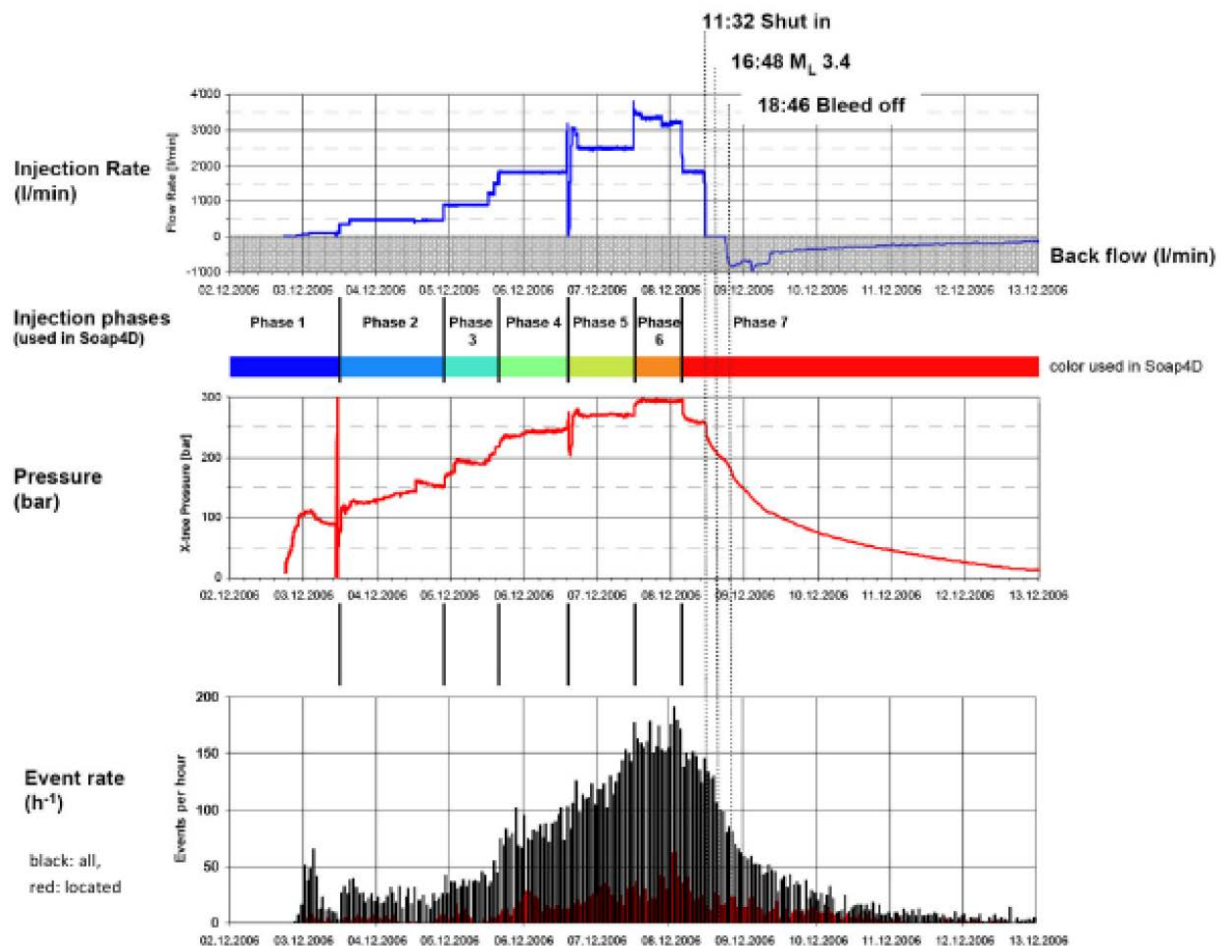

Fig. 4.3: Injection rate, injection phases, wellhead pressure and quake number during stimulation of borehole Basel-1 (Delacou & Sartori, 2009)

The induced seismicity is still one of the major problems hindering the use of deep geothermal energy (e.g. Vasteling et al., 2017, Kwiatek et al., 2019). Fig. 4.4 shows localization results of injection induced seismicity during stimulation processes in a

Dynamic events in rocks / rockmasses

Only for private and internal use!   Updated: 16 September 2021

deep geothermal well in Finland. A correlation between injected volume and magnitude and seismic moment is observed, respectively (see Fig. 4.5).
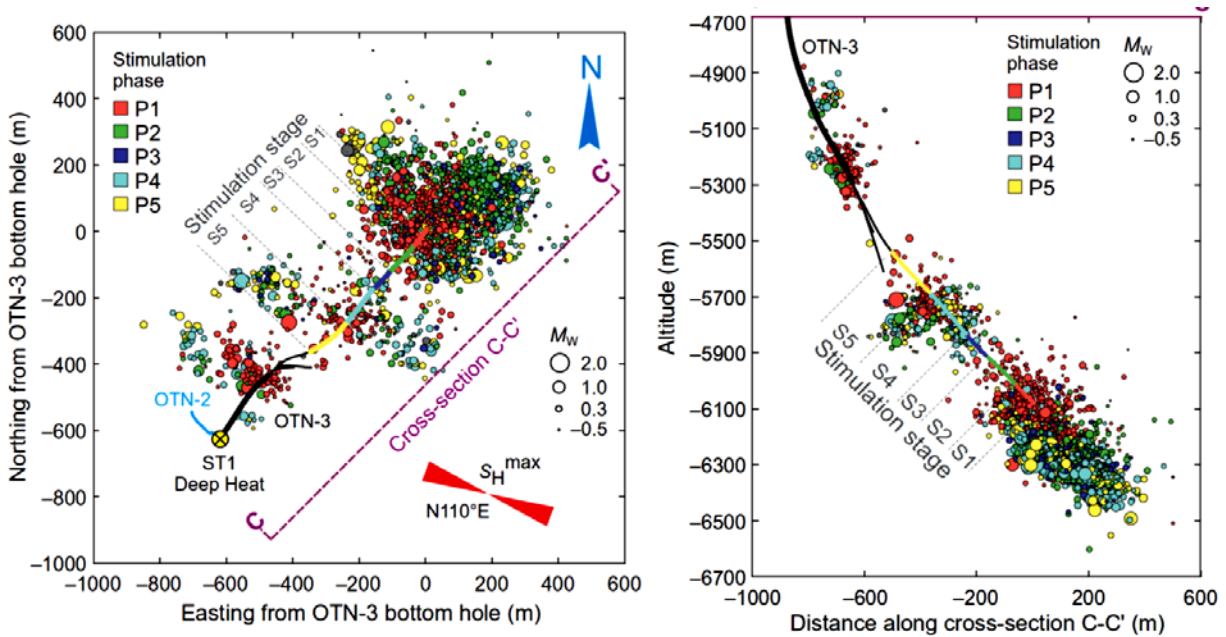

Fig. 4.4: Localization of induced seismicity during stimulation in borehole OTN-3 (Kwiatek et al., 2019)
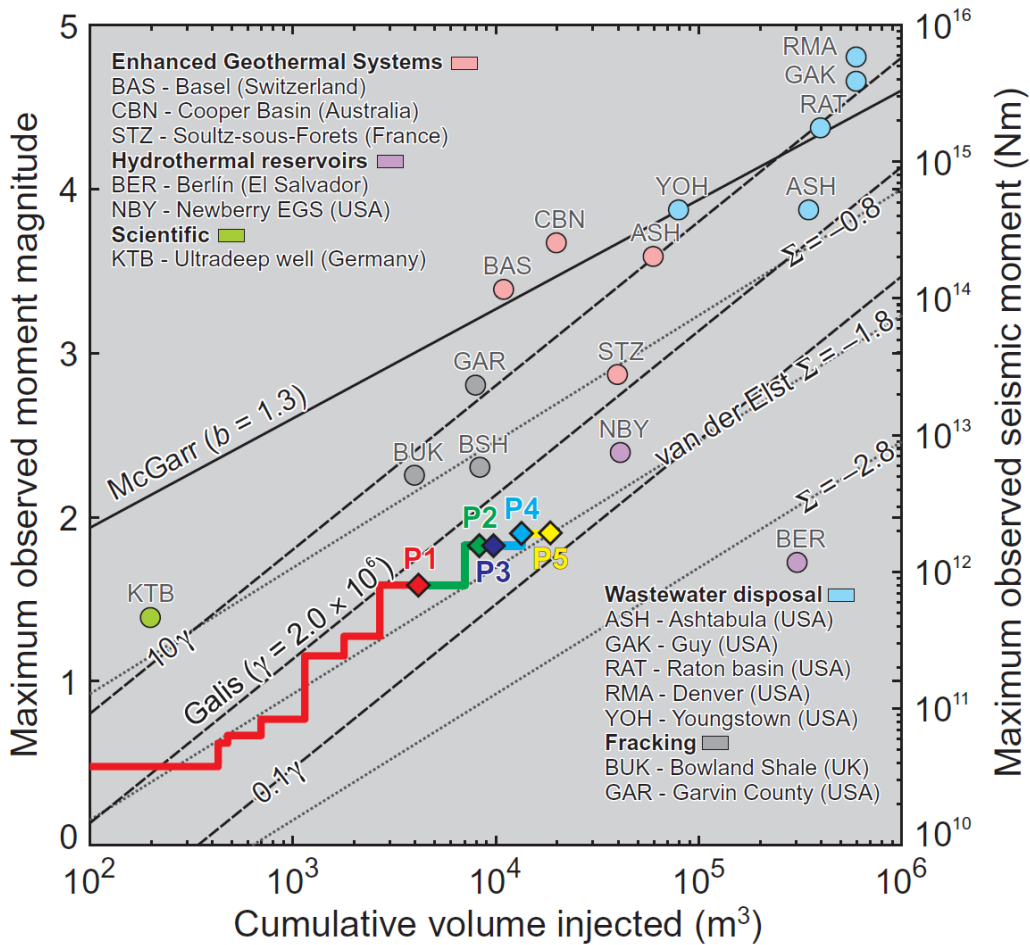

Fig. 4.5: Temporal evolution of maximum observed seismic moment versus cumulative volume of injected fluid at each phase (P1 to P5) for borehole OTN-3 (Kwiatek et al., 2019)

5   Scaling laws

Scaling laws describe empirical relations between different fundamental quantities in seismology and engineering seismology, respectively. They allow to estimate unknown quantities on the basis of measured or known parameters. Such relations are deduced on the basis of a large amount of monitoring data. They are valid only for specific constellations and specific parameter ranges. Scaling laws are given as formulas or graphs. Typical parameters considered in scaling laws are:

- Different types of magnitude
- Seismic moments
- Intensities
- Accelerations
- Vibration velocities
- Duration of vibration
- Source parameters like source dimension, stress drop, slip

Several scaling laws are provided for instance by Hurtig and Stiller (1984), Bormann (2011), Grünthal (2011), Thingbaijam et al. (2017) or Caprio et al. (2015).

Exemplary, Fig. 5.1 shows a scaling for different types of magnitude, Fig. 5.2 shows relations between the intensity and peak ground acceleration and velocity. Fig. 5.3 shows a relation between rupture area and magnitude.
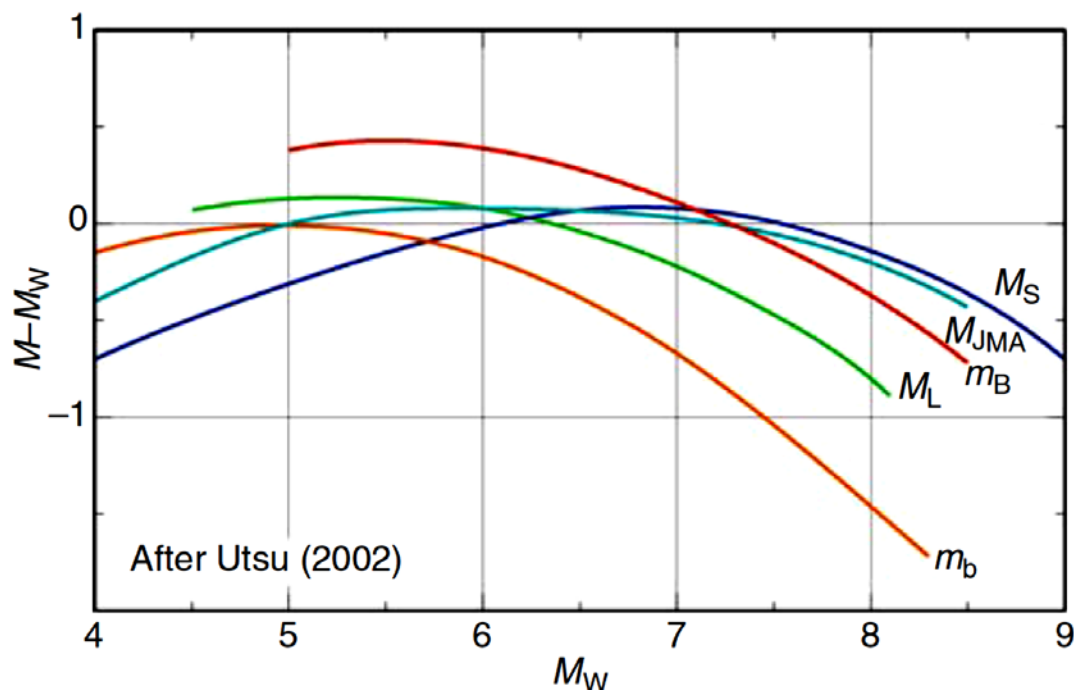

Fig. 5.1: Relation between different types of magnitude: m_b = body wave magnitude, M_L= local magnitude, M_W = moment magnitude, M_{JMA} = magnitude by JMA, M_S = surface wave magnitude (Bormann, 2011)
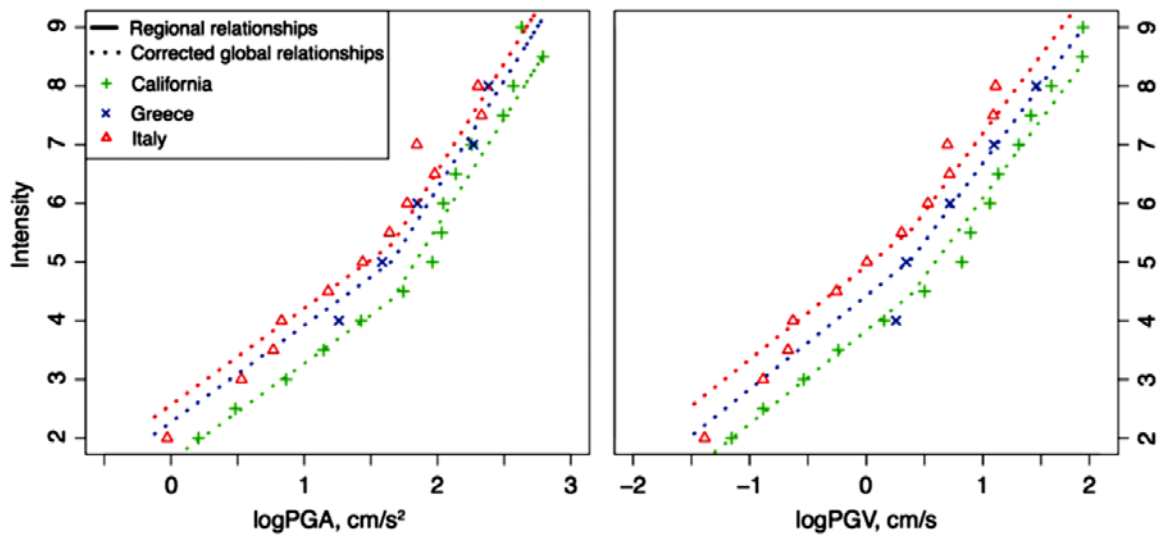
Fig. 5.2: Scaling laws for intensity, peak ground acceleration and peak ground velocities (Caprio et al., 2015)
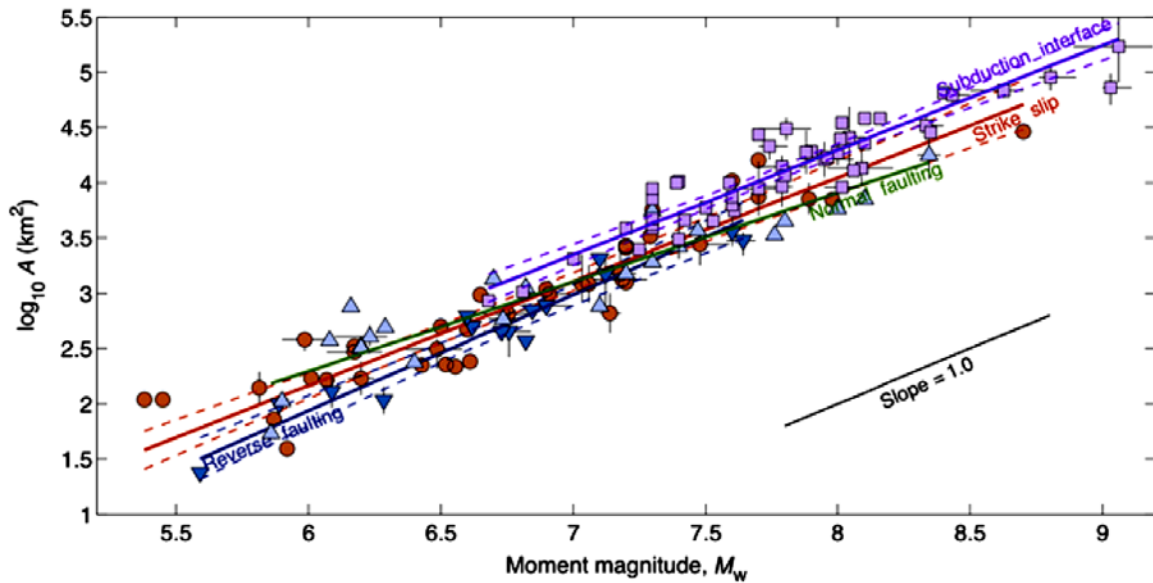

Fig. 5.3: Scaling law: moment magnitude vs. rupture area (Thingbaijam et al., 2017)

Dynamic events in rocks / rockmasses

Only for private and internal use!   Updated: 16 September 2021

6 Blast vibrations

Blasts are used in many geotechnical applications like at:

- hard rock open-cast mining (basalt, granite, diabase etc.),
- underground mining (coal, salt, ores etc.),
- traffic route engineering,
- tunnel construction and
- seismic exploration methods.

During detonation explosion gases are generated. Due to the high explosion pressure the gas is compressed and increases the gas pressure. The pressure change is approximately

$$\Delta p = \frac{p_1}{p_2} = \left(\frac{V_2}{V_1}\right)^K \tag{5.1}$$

Thereby K is the gas rigidity factor and is usually K ≈ 3. The detonation velocity v_{det} can be estimated as follows:

$$v_{det} = \sqrt{2\left(K^2 - 1\right)U \cdot g} \tag{5.2}$$

g denotes the gravity acceleration and U the specific explosion energy. The detonation velocity reaches several km/s depending on the blasting force. The detonation pressure p_{det} can be assessed via the explosive density ρ as follows:

$$p_{det} = 2\left(K - 1\right)\rho \cdot U \cdot g \tag{5.3}$$

The order of p_{det} lies in the range of GPa.

The cavity radius R can be estimated empirically using the explosive charge quantity q (in kg).

$$R_K = 0.1 \sim 0.4 \cdot \sqrt[3]{q} \cdot \left[\frac{m}{\sqrt[3]{kg}}\right] \tag{5.4}$$

The size of the corresponding pressure destruction zone is nearly $R_D \approx 2R_K$ and the size of the fractured zone $R_R \approx 4R_K$.

The fracture patterns for homogeneous full and half space are illustrated in Fig. 5.1.

Dynamic events in rocks / rockmasses

Only for private and internal use!   Updated: 16 September 2021
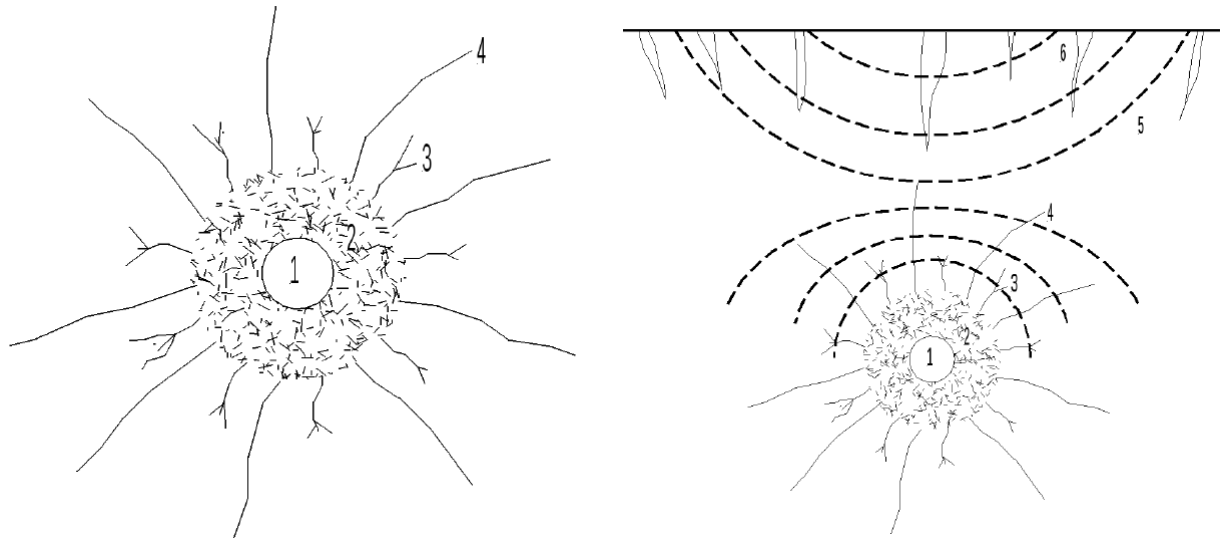

Fig. 5.1: Fracture patterns for homogeneous full and half space (source: Jendersie et al. 1981)

1. borehole
2. pressure destruction
3. radial cracks
4. extention of radial cracks and (at half space:) tangential cracks from decompression wave
5. tangential cracks from reflected tension wave
6. radial cracks near surface from compression and tension waves

Dynamic events in rocks / rockmasses

Only for private and internal use!   Updated: 16 September 2021

References

Aso, N. et al. (2016): Mathematical review on source-type diagrams, Earth, Planets and Space, 68:52

Berckhemer, H. (1990): Grundlagen der Geophysik. Darmstadt: Wissenschaftliche Buchgessellschaft, ISBN: 3-534-03974-2.

Bormann, P. (2011): Earthquake magnitude, in: Gupta, H.K.: Encyclopedia of solid earth geophysics, 207- 218, Springer.

Caprio, M. et al. (2015): Ground motion to intensity conversion equation (GMICEs): a global relationship and evaluation of regional dependency, Bull. Seismological Society, 105(3): 1-15

Delacou, B. & Sartori M. (2009): AP2000 Report - Structural model of potential seismogenic faults. Bureau d'Etudes Géologiques SA.

Dusseault, M. B. et al. (2001): Casing Shear: Causes, Cases, Cures, SPE Drilling & Completion 16(2): 98–107.

Evans, K. F. et al. (2012): A survey of the induced seismic responses to fluid injection in geothermal and CO_2 reservoirs in Europe. Geothermics 41: 30–54.

Fischer, T. & Horálek, J. (2000): Refined locations of the swarm earthquakes in the Novy Kostel focal zone and spatial distribution of the January 1997 swarm in Western Bohemia, Czech Republic, Studia Geophysica et Geodætica, 44(2): 210–226.

Grünthal, G. (1981): Zur Seismizität des Territoriums der DDR, Gerlands Beiträge zur Geophysik 90(3): 202–212.

— (2004). Erdbeben und Erdbebengefährdung in Deutschland sowie im europäischen Kontext, Geographie und Schule, 151: 14–23.

Grünthal, G. & Minkley, W. (2005): Bergbauinduzierte seismische Aktivitäten als Quelle seismischer Belastungen - Zur Notwendigkeit der Ergänzung der Karte der Erdbebenzonen der DIN 4149:2005-04, Bautechnik 82(8): 508–513.

Grünthal, G. (2011): Earthquake intensity, in: Gupta, H.K.: Encyclopedia of solid earth geophysics, 237-242, Springer.

Gupta, H. K. (1992): Reservoir-Induced Earthquakes, Elsevier.

Hurtig, E. (1984): Erdbeben und Erdbebengefährdung, Berlin: Akademie-Verlag

Jakob, C. (2009): Herdparameterbestimmung von Erdbeben zur seismotektonischen Analyse in der Schwarmbebenregion Vogtland/NW-Böhmen. Diplomarbeit. TU Bergakademie Freiberg.

Jendersie, H. et al. (1981): Sprengtechnik im Bergbau, Leipzig: Deutscher Verlag für Grundstoffindustrie.

Künzel, U. (2013): Seismizität im Umfeld der Uranerzlagerstätte Schlema-Alberoda und modifizierte Auswertemethoden für eine präzise Lage- und Stärkeermittlung der im Nahfeld instrumentell registrierten Mikrobeben. Ed. Konietzky, H., Institut für Geotechnik der TU Bergakademie Freiberg.

Kwiatek, G. et al. (2019): Controlling fluid-induced seismicity during a 6.1-km-deep geothermal stimulation in Finland, Science Advances, 5: eaav7224.

Madariaga, R. (1976): Dynamics of an expanding circular fault, Bull. Seismological Society of America 66(3): 639–666.

mxrap (2021): https://mxrap.com/moment-tensors-a-practical-guide.

Schulte-Theis, H. (1995): Automatische Lokalisierung und Clusteranalyse regionaler Erdbeben, Dissertation, Ruhr-Universität Bochum.

Schütz, H. & Konietzky, H. (2016): Evaluation of flooding induced seismicity from the mining area Schlema/Alberoda (Germany). Rock Mechanics Rock Engineering, 49: 4125-4135.

Seed, H. B. et al. (Dec. 1974): Site-dependent spectra for earthquake-resistant design. Tech. rep. EERC-Rep.

Simpson, D. W. (1976): Seismicity changes associated with reservoir loading, Engineering Geology 10: 123–150.

Studer, J. A. & Koller, M.G. (1997): Geotechnisches Erdbebeningenieurwesen. German. In: Bodendynamik. Springer Berlin Heidelberg, 224–322.

Thingbaijam, K.K.S. et al. (2017): New empirical earthquake source-scaling laws, Bull. Seismological Society, 107(5): 2225-2246.

Vasterling, M. et al. (2017): Real-time envelope cross-correlation detector: application to induced seismicity in the Insheim and landau deep geothermal reservoirs, J. Seismology, 21: 193-208.

Vavrycuk, V. (2015): Moment tensor decompositions revisited, J. Seismology, 19: 231-252.

Waldhauser, F. (2010): hypoDD – A Program to Compute Double-Difference Hypocentre Locations. Manual.